arXiv:1411.3598v1 [math-ph] 13 Nov 2014

First Exit Times of Harmonically Trapped Particles: A Didactic Review

Denis S. Grebenkov

E-mail: denis.grebenkov@polytechnique.edu
[1] Laboratoire de Physique de la Matière Condensée (UMR 7643),
CNRS – Ecole Polytechnique, 91128 Palaiseau, France
[2] St. Petersburg National Research University of Information Technologies,
Mechanics and Optics, 197101 St. Petersburg, Russia

Abstract. We revise the classical problem of characterizing first exit times of a harmonically trapped particle whose motion is described by one- or multi-dimensional Ornstein-Uhlenbeck process. We start by recalling the main derivation steps of a propagator using Langevin and Fokker-Planck equations. The mean exit time, the moment-generating function, and the survival probability are then expressed through confluent hypergeometric functions and thoroughly analyzed. We also present a rapidly converging series representation of confluent hypergeometric functions that is particularly well suited for numerical computation of eigenvalues and eigenfunctions of the governing Fokker-Planck operator. We discuss several applications of first exit times such as detection of time intervals during which motor proteins exert a constant force onto a tracer in optical tweezers single-particle tracking experiments; adhesion bond dissociation under mechanical stress; characterization of active periods of trend following and mean-reverting strategies in algorithmic trading on stock markets; relation to the distribution of first crossing times of a moving boundary by Brownian motion. Some extensions are described, including diffusion under quadratic double-well potential and anomalous diffusion.

PACS numbers: 02.50.Ey, 05.10.Gg, 05.40.-a, 02.30.Gp

Keywords: first exit time; first passage time; survival probability; harmonic potential; double-well potential; Ornstein-Uhlenbeck process; confluent hypergeometric function; Kummer and Tricomi functions; parabolic cylinder function; optical tweezers; quantum harmonic oscillator

Submitted to: *J. Phys. A: Math. Gen.*

Contents

1 Introduction **2**

2 First exit time distribution **3**
2.1 Langevin equation 4
2.2 Forward Fokker-Planck equation 5
2.3 Backward Fokker-Planck equation 7
2.4 First exit times 8
2.5 Mean exit time 10
2.6 Survival probability 13
2.7 Moment-generating function 16
2.8 Higher-dimensional case 17
2.9 Exterior problem 19
2.10 Similarities and distinctions 22

3 Discussion **23**
3.1 Computational hints 23
3.2 Single-particle tracking 24
3.3 Adhesion bond dissociation under mechanical stress 26
3.4 Algorithmic trading 27
3.5 First crossing of a moving boundary by Brownian motion 28
3.6 Quadratic double-well potential 29
3.7 Further extensions 31

Conclusion **32**

Appendices **33**

References **43**

1. Introduction

First passage time (FPT) distributions have found numerous applications in applied mathematics, physics, biology and finance [1, 2, 3]. The FPT can characterize the time needed for an animal to find food; the time for an enzyme to localize specific DNA sequence and to initiate biochemical reaction; the time to exit from a confining domain (e.g., a maze); or the time to buy or sell an asset when its price deviation from the mean exceeds a prescribed threshold. The FPT distribution has been studied for a variety of diffusive processes, ranging from ordinary diffusion (Brownian motion) to continuous-time random walks (CTRWs) [4, 5, 6, 7, 8, 9, 10, 11], fractional Brownian motion [12, 13, 14, 15], Lévy flights [16, 17, 18], surface-mediated diffusion [19, 20, 21, 22] and other intermittent processes [23, 24], diffusion in scale

invariant media [25, 26], trapped diffusion [27], thermally driven oscillators [28], Ornstein-Uhlenbeck process [29, 30, 31, 32, 33, 34, 35, 36, 37, 38], and many others [1, 2, 39, 40, 41, 42, 43, 44, 45, 46, 47, 48].

In this review, we revise the classical problem of characterizing the first *exit* time (FET) distribution of a multi-dimensional Ornstein-Uhlenbeck process from a ball [49, 50, 51]. The probability distribution can be found through the inverse Fourier (resp. Laplace) transform of the characteristic (resp. moment-generating) function for which explicit representations in terms of special functions are well known [30, 39]. Although the problem is formally solved, the solution involves confluent hypergeometric functions and thus requires subtle asymptotic methods and computational hints. The aim of the review is to provide a didactic self-consistent description of theoretical, numerical and practical aspects of this problem.

First, we recall the main derivation steps of the FET distribution, from the Langevin equation (Sec. 2.1), through forward and backward Fokker-Planck (FP) equations (Sec. 2.2, 2.3), to spectral decompositions based on the eigenvalues and eigenfunctions of the FP operator (Sec. 2.4). This general formalism is then applied to describe the first exit times of harmonically trapped particles in one dimension: the mean exit time (Sec. 2.5), the survival probability (Sec. 2.6), and the moment-generating function (Sec. 2.7). In particular, we analyze the asymptotic behavior of the mean exit time and eigenvalues in different limits (e.g., strong trapping potential, large constant force, etc.). Extensions to the radial Ornstein-Uhlenbeck process in higher-dimensional cases for both interior and exterior problems are presented in Sec. 2.8 and Sec. 2.9, respectively. Although most of these results are classical, their systematic self-contained presentation and numerical illustrations are missing.

Section 3 starts from the summary of computational hints for computing confluent hypergeometric functions while technical details are reported in Appendix B. We discuss then three applications: (i) calibration of optical tweezers' stiffness in single-particle tracking experiments and detection of eventual constant forces exerted on a tracer by motor proteins (Sec. 3.2), (ii) adhesion bond dissociation under mechanical stress (Sec. 3.3), and (iii) distribution of triggering times of trend following strategies in algorithmic trading on stock markets (Sec. 3.4). We also illustrate a direct relation to the distribution of first crossing times of a moving boundary by Brownian motion (Sec. 3.5). Finally, we present several extensions of the spectral approach, including diffusion under quadratic double-well potential (Sec. 3.6) and anomalous diffusion (Sec. 3.7). Many technical details are summarized in Appendices.

2. First exit time distribution

We first recall the standard theoretical description of harmonically trapped particles by Langevin and Fokker-Planck equations [46, 52, 53]. We start with one-dimensional Ornstein-Uhlenbeck process and then discuss straightforward extensions to higher dimensions.

2.1. Langevin equation

We consider a diffusing particle of mass m trapped by a harmonic potential of strength k and pulled by a constant force F_0. The thermal bath surrounding the particle results in its stochastic trajectory which can be described by Langevin equation [52]

$$m\ddot{X}(t) = -\gamma\dot{X}(t) + F(X(t)) + \xi(t), \tag{1}$$

where $-\gamma\dot{X}(t)$ is the viscous Stokes force (γ being the drag constant), $F(X(t)) = -kX(t) + F_0$ includes the externally applied Hookean and constant forces, and $\xi(t)$ is the thermal driving force with Gaussian distribution such that $\langle\xi(t)\rangle = 0$ and $\langle\xi(t)\xi(t')\rangle = 2k_BT\gamma\delta(t-t')$, with $k_B \simeq 1.38\cdot10^{-23}\ J/K$ being the Boltzmann constant, T the absolute temperature (in degrees Kelvin), $\delta(t)$ the Dirac distribution, and $\langle\ldots\rangle$ denoting the ensemble average or expectation. In the overdamped limit ($m = 0$), one gets the first-order stochastic differential equation

$$\dot{X}(t) = \frac{1}{\gamma}[F(X(t)) + \xi(t)] = \frac{k}{\gamma}(\hat{x} - X(t)) + \frac{\xi(t)}{\gamma}, \qquad X(0) = x_0, \tag{2}$$

where $\hat{x} = F_0/k$ is the stationary position (mean value), and x_0 is the starting position. The Langevin equation can also be written in a conventional (dimensionless) stochastic form [39, 40]

$$dX_t = \mu(X_t, t)dt + \sigma(X_t, t)dW_t, \qquad X_0 = x_0, \tag{3}$$

where W_t is the standard Wiener process (Brownian motion), $\mu(x,t)$ and $\sigma(x,t)$ are the drift and volatility which in general can depend on x and t. In our case, the volatility is constant, while the drift is a linear function of x, $\mu(x,t) = (\hat{x} - x)\theta$, i.e.

$$dX_t = \theta(\hat{x} - X_t)dt + \sigma dW_t, \qquad X_0 = x_0, \tag{4}$$

where $\theta = k\delta/\gamma$, and $\sigma = \sqrt{2D\delta}$, with δ being a time scale, and $D = k_BT/\gamma$ the diffusion coefficient. This stochastic differential equation defines an Ornstein-Uhlenbeck (OU) process, with mean $\hat{x}$, variance σ^2, and rate θ. An integral representation of Eq. (4) reads

$$X_t = x_0e^{-\theta t} + \hat{x}(1 - e^{-\theta t}) + \sigma\int_0^t e^{\theta(t'-t)}dW_{t'}. \tag{5}$$

One can see that X_t is a Gaussian process with mean $\langle X_t\rangle = x_0e^{-\theta t} + \hat{x}(1 - e^{-\theta t})$ and covariance $\langle X_tX_{t'}\rangle = \frac{\sigma^2}{2\theta}(e^{-\theta|t-t'|} - e^{-\theta(t+t')})$.

The discrete version of Eq. (4) with a fixed time step δ is known as auto-regressive model AR(1):

$$X_n = (1 - k\delta/\gamma)X_{n-1} + F_0\delta/\gamma + \sqrt{2D\delta}\ \xi_n, \tag{6}$$

where ξ_n are standard iid Gaussian variables with mean zero and unit variance. This discrete scheme can be used for numerical generation of stochastic trajectories. An extension of the above stochastic description to multi-dimensional processes is straightforward.

2.2. Forward Fokker-Planck equation

The Langevin equation (2) expresses the displacement $\dot{X}(t)\delta$ over a short time step δ in terms of the current position $X(t)$. In other words, the distribution of the next position is fully determined by the current position, the so-called Markov property. Such a Markov process can be characterized by a propagator or a transition density, i.e., the conditional probability density $p(x,t|x_0,t_0)$ of finding the particle at x at time t, given that it was at x_0 at earlier time t_0. The propagator can be seen as a "fraction" of paths from x_0 to x among all paths started at x_0 (of duration $t-t_0$) which formally writes as the average of the Dirac distribution $\delta(X(t)-x)$ over all random paths started from x_0: $p(x,t|x_0,t_0) = \langle \delta(X(t)-x)\rangle_{X(t_0)=x_0}$. The Markov property implies the Chapman-Kolmogorov (or Smoluchowski) equation

$$p(x,t|x_0,t_0) = \int_{-\infty}^{\infty} dx'\; p(x,t|x',t')\; p(x',t'|x_0,t_0) \qquad (t_0<t'<t), \tag{7}$$

which expresses a simple fact that any continuous path from $X(t_0)=x_0$ to $X(t)=x$ can be split at any intermediate time t' into two *independent* paths, from x_0 to x', and from x' to x.

As a function of the arrival state (x and t), the propagator satisfies the forward Fokker-Planck (FP) equation [52, 53]. We reproduce the derivation of this equation from [54] which relies on the evaluation of the integral

$$I = \int_{-\infty}^{\infty} dx\; h(x)\Big[p(x,t+\delta|x_0,t_0) - p(x,t|x_0,t_0)\Big]$$

for any smooth function $h(x)$ with compact support. One has

$$\begin{aligned} I = &\int_{-\infty}^{\infty} dx\; h(x) \int_{-\infty}^{\infty} dx'\; p(x,t+\delta|x',t)\; p(x',t|x_0,t_0) \\ &- \int_{-\infty}^{\infty} dx'\; h(x')\; p(x',t|x_0,t_0) \int_{-\infty}^{\infty} dx\; p(x,t+\delta|x',t) \\ = &\int_{-\infty}^{\infty} dx \int_{-\infty}^{\infty} dx'\; p(x,t+\delta|x',t)\; p(x',t|x_0,t_0)\; \Big[h(x)-h(x')\Big], \end{aligned}$$

where the first term was represented using Eq. (7), while the normalization of the probability density $p(x,t+\delta|x',t)$ allowed one to add the integral over x in the second term. Expanding $h(x)$ into a Taylor series around x' and then exchanging the integration variables x and x', one gets

$$I = \int_{-\infty}^{\infty} dx\; p(x,t|x_0,t_0)\; \sum_{n=1}^{\infty} \left(\frac{d^n}{dx^n}h(x)\right)\; \frac{1}{n!} \int_{-\infty}^{\infty} dx'\; p(x',t+\delta|x,t)\; (x'-x)^n,$$

Finally, integrating each term by parts n times, dividing by δ and taking the limit $\delta \to 0$ yield

$$\int_{-\infty}^{\infty} dx\ h(x)\ \frac{\partial p(x,t|x_0,t_0)}{\partial t} = \int_{-\infty}^{\infty} dx\ h(x) \sum_{n=1}^{\infty} (-1)^n \frac{d^n}{dx^n}\Big(D^{(n)}(x)\ p(x,t|x_0,t_0)\Big),$$

where the left hand side is the limit of I/δ as $\delta \to 0$, and

$$D^{(n)}(x) = \frac{1}{n!} \lim_{\delta\to 0} \frac{1}{\delta} \int_{-\infty}^{\infty} dx'\ p(x', t+\delta|x,t)\ (x'-x)^n. \tag{8}$$

Since the above integral relation is satisfied for arbitrary function $h(x)$, one deduces the so-called Kramers-Moyal expansion:

$$\frac{\partial p(x,t|x_0,t_0)}{\partial t} = \sum_{n=1}^{\infty} (-1)^n \frac{d^n}{dx^n}\Big(D^{(n)}(x)\ p(x,t|x_0,t_0)\Big). \tag{9}$$

Here we assumed that the process is time homogeneous, i.e., $p(x,t|x_0,t_0)$ is invariant under time shift: $p(x,t|x_0,t_0) = p(x,t+t'|x_0,t_0+t')$ that implies the time-independence of $D^{(n)}(x)$.

The density $p(x', t+\delta|x,t)$ in Eq. (8) characterizes the displacement between $X(t) = x$ and $X(t+\delta) = x'$ which can be written as $X(t+\delta) - X(t) \simeq \frac{\delta}{\gamma}[F(x) + \xi(t)]$ for small δ according to the Langevin equation (2). After discretization in units of δ, the thermal force $\xi(t)$ becomes a Gaussian variable with mean zero and variance $2k_BT\gamma/\delta$. As a consequence, the displacement $x' - x$ is also a Gaussian variable with mean $(\delta/\gamma)F(x)$ and variance $(\delta/\gamma)^2\ 2k_BT\gamma/\delta$, i.e.,

$$p(x', t+\delta|x,t) = \frac{1}{\sqrt{4\pi D\delta}} \exp\left(-\frac{(x'-x-F(x)\delta/\gamma)^2}{4D\delta}\right)$$

for small δ. Substituting this density into Eq. (8) and evaluating Gaussian integrals, one gets $D^{(1)}(x) = F(x)/\gamma$, $D^{(2)} = D$, and $D^{(n)} = 0$ for $n > 2$ that yields the forward Fokker-Planck equation

$$\frac{\partial}{\partial t}\ p(x,t|x_0,t_0) = Ł_x\ p(x,t|x_0,t_0), \qquad Ł_x = -\partial_x \frac{F(x)}{\gamma} + D\partial_x^2, \tag{10}$$

where $Ł_x$ is the Fokker-Planck operator acting on the arrival point x. This equation is completed by the initial condition $p(x,t_0|x_0,t_0) = \delta(x-x_0)$ at $t = t_0$, with a fixed starting point x_0. Note that the forward FP equation can be seen as the probability conservation law,

$$\frac{\partial}{\partial t}\ p(x,t|x_0,t_0) = -\partial_x J(x,t|x_0,t_0),$$

where $J(x,t|x_0,t_0) = \frac{F(x)}{\gamma} p(x,t|x_0,t_0) - D\partial_x p(x,t|x_0,t_0)$ is the probability flux. Setting $J = 0$, one can solves the first-order differential equation to retrieve the equilibrium solution $p_{\rm eq}(x) = Zw(x)$, where Z is the normalization factor, and

$$w(x) = \exp\left(\int_0^x dx' \frac{F(x')}{k_BT}\right) = \exp\left(-\frac{V(x)}{k_BT}\right) = \exp\left(-\frac{kx^2}{2k_BT} + \frac{F_0 x}{k_BT}\right), \tag{11}$$

where $V(x) = -\int_0^x dx' F(x')$ is the potential associated to the force $F(x)$. This is the standard Boltzmann-Gibbs equilibrium distribution.

When the FP operator $Ł_x$ has a discrete spectrum, the probability density admits the spectral decomposition

$$p(x,t|x_0,t_0) = \sum_{n=0}^{\infty} v_n(x)\ v_n(x_0)\ \tilde{w}(x_0)\ e^{-\lambda_n(t-t_0)} \tag{12}$$

over the eigenvalues λ_n and eigenfunctions $v_n(x)$ of $Ł_x$:

$$Ł_x v_n(x) + \lambda_n v_n(x) = 0 \qquad (n = 0, 1, 2, \ldots) \tag{13}$$

(eventually with appropriate boundary conditions, see below). The weight $\tilde{w}(x) = 1/w(x)$ ensures the orthogonality of eigenfunctions:

$$\int dx\ \tilde{w}(x)\ v_m(x)\ v_n(x) = \delta_{m,n}, \tag{14}$$

while the closure (or completeness) relation reads

$$\sum_{n=0}^{\infty} v_n(x)\ v_n(x_0)\ \tilde{w}(x_0) = \delta(x - x_0). \tag{15}$$

This relation implies the initial condition $p(x,t_0|x_0,t_0) = \delta(x-x_0)$. As for the Langevin equation, an extension to the multi-dimensional case is straightforward. In particular, the derivative ∂_x is replaced by the gradient operator, while ∂_x^2 becomes the Laplace operator [53, 55].

2.3. Backward Fokker-Planck equation

The forward FP equation describes the evolution of the probability density $p(x,t|x_0,t_0)$ from a given initial state (here, the starting point x_0 at time t_0). Alternatively, if the particle is found at the arrival point x at time t (or, more generally, in a prescribed subset of states), one can interpret $p(x,t|x_0,t_0)$ as the conditional probability density that the particle is started from x_0 at time t_0 knowing that it arrived at x at later time t. As a function of x_0 and t_0, this probability density satisfies the *backward* Fokker-Planck (or Kolmogorov) equation [53]:

$$-\frac{\partial}{\partial t_0}\ p(x,t|x_0,t_0) = Ł^*_{x_0}\ p(x,t|x_0,t_0), \tag{16}$$

where the backward FP operator $Ł^*$ is adjoint to the forward FP operator $Ł$ (i.e., $(Łf, g) = (f, Ł^* g)$ for any two functions f and g from an appropriate functional space). Eq. (10) implies

$$Ł^*_{x_0} = \frac{F(x_0)}{\gamma}\partial_{x_0} + D\partial^2_{x_0} = \frac{k}{\gamma}(\hat{x} - x_0)\partial_{x_0} + D\partial^2_{x_0}. \tag{17}$$

Note that this operator acts on the starting point x_0 while the sign minus in front of time derivative reflects the backward time direction. Eq. (16) is easily obtained by differentiating the Champan-Kolmogorov equation (7) with respect to the intermediate time t'.

The eigenvalues of both forward and backward FP operators are identical, while the eigenfunctions $u_n(x)$ of the backward FP operator $Ł^*$ are simply $u_n(x) = v_n(x)/w(x)$. As a consequence, one can rewrite the spectral decomposition (12) as

$$p(x,t|x_0,t_0) = \sum_{n=0}^{\infty} u_n(x_0)\ u_n(x)\ w(x)\ e^{-\lambda_n(t-t_0)}, \tag{18}$$

with the weight $w(x)$ from Eq. (11). The eigenfunctions $u_n(x)$ are as well orthogonal:

$$\int dx\ w(x)\ u_m(x)\ u_n(x) = \delta_{m,n}, \tag{19}$$

while the closure (or completeness) relation reads

$$\sum_{n=0}^{\infty} u_n(x_0)\ u_n(x)\ w(x) = \delta(x-x_0). \tag{20}$$

This relation implies the terminal condition $p(x,t|x_0,t) = \delta(x-x_0)$ at $t_0 = t$. In contrast to Eq. (12), the weight $w(x)$ in the spectral representation (18) depends on the *fixed* arrival point x, while the backward FP operator $Ł^*_{x_0}$ acts on eigenfunctions $u_n(x_0)$.

When there is no force term, the operator Ł is self-adjoint, Ł = $Ł^*$, and the probability density is invariant under time reversal: $p(x,t|x_0,t_0) = p(x_0,t_0|x,t)$. This property does not hold in the presence of force.

Finally, the backward FP equation is closely related to the Feynman-Kac formula for determining distributions of various Wiener functionals [56, 57, 58, 59, 60]. For instance, we already mentioned that the probability density $p(x,t|x_0,t_0)$ can be understood as the conditional expectation: $p(x,t|x_0,t_0) = \langle \delta(X(t)-x)\rangle_{X(t_0)=x_0}$. More generally, for given functions $\psi(x_0)$, $f(x_0,t_0)$ and $U(x_0,t_0)$, the conditional expectation

$$\begin{aligned} u(x_0,t_0) = \Big\langle \exp\Big(-\int_{t_0}^{t} dt' U(X(t'),t')\Big)\psi(X(t)) \\ + \int_{t_0}^{t} dt' f(X(t'),t') \exp\Big(-\int_{t_0}^{t'} dt'' U(X(t''),t'')\Big)\Big\rangle_{X(t_0)=x_0} \end{aligned} \tag{21}$$

satisfies the backward FP equation

$$-\frac{\partial}{\partial t_0} u(x_0,t_0) = Ł^*_{x_0} u(x_0,t_0) - U(x_0,t_0)u(x_0,t_0) + f(x_0,t_0), \tag{22}$$

subject to the terminal condition $u(x_0,t) = \psi(x_0)$ at a later time $t > t_0$.

2.4. First exit times

In this review, we study the random variable $\tau = \inf\{t > 0\ :\ |X(t)| > L\}$, i.e., the first exit time of the process $X(t)$ from an interval $[-L,L]$ when started from x_0 at $t_0 = 0$. The cumulative distribution function of τ is also known as the survival probability $S(x_0,t) = \mathbb{P}\{\tau > t\}$ up to time t of a particle which started from x_0. The notion of *survival* is associated to disappearing of the particle that hit either endpoint, due

to chemical reaction, permeation, adsorption, relaxation, annihilation, transformation or any other "killing" mechanism. The survival probability $S(x_0,t)$ can be expressed through the probability density $p(x,t|x_0,0)$ of moving from x_0 to x in time t *without visiting the endpoints* $\pm L$ *during this motion*. Alternatively, $p(x,t|x_0,0)$ can be seen as the conditional probability density of starting from point x_0 at time $t_0=0$ under condition to be at x at time t. This condition includes the survival up to time t, i.e., not visiting the endpoints $\pm L$. The probability density $p(x,t|x_0,0)$ satisfies the backward FP equation with Dirichlet boundary condition at $x_0=\pm L$: $p(x,t|\pm L,0)=0$. This condition simply states that a particle started from either endpoint has immediately hit this endpoint, i.e. not survived. Note that this condition is preserved during all intermediate times t' due to the Chapman-Kolmogorov equation (7).

Since the survival probability $S(x_0,t)$ ignores the actual position x at time t, one just needs to average the density $p(x,t|x_0,0)$ over x:

$$S(x_0,t)=\int\limits_{-L}^{L} dx\; p(x,t|x_0,0)=\sum_{n=0}^{\infty} u_n(x_0)\; e^{-\lambda_n t}\int\limits_{-L}^{L} dx\; u_n(x)w(x), \tag{23}$$

where the spectral decomposition (18) was used. The eigenfunctions $u_n(x)$ of the backward FP operator should satisfy Dirichlet boundary condition at $x_0=\pm L$: $u_n(\pm L)=0$. Eq. (23) also implies the backward FP equation

$$\frac{\partial S(x_0,t)}{\partial t}=Ł^*_{x_0}S(x_0,t), \tag{24}$$

which is completed by the initial condition $S(x_0,0)=1$ (the particle exists at the beginning) and Dirichlet boundary condition $S(\pm L,t)=0$ (the process is stopped upon the first arrival at either endpoint of the confining interval $[-L,L]$). Since the process is homogeneous in time, $p(x,t|x_0,t_0)$ depends on $t-t_0$ and thus $\frac{\partial}{\partial t_0}p(x,t|x_0,t_0)=-\frac{\partial}{\partial t}p(x,t|x_0,t_0)$ that allows one to write the left-hand side of the backward FP equation (24) with the plus sign. Note that the characterization of first passage times through the backward FP equation goes back to the seminal work in 1933 by Pontryagin *et al.* [61]. Similar equations emerge in quantum mechanics when one searches for eigenstates of a particle trapped by a short-range harmonic potential [62] (see also Appendix D for quantum harmonic oscillator).

The FET probability density is $q(x_0,t)=-\frac{\partial S(x_0,t)}{\partial t}$, while the moment-generating function is given by its Laplace transform:

$$\langle e^{-s\tau}\rangle=\int\limits_0^{\infty} dt\; e^{-st}q(x_0,t)\equiv\tilde{q}(x_0,s), \tag{25}$$

with tilde denoting Laplace-transformed quantities. The Laplace transform of Eq. (24) yields the equation $(Ł^*_{x_0}-s)\tilde{S}(x_0,s)=-1$ with Dirichlet boundary conditions. Since $\tilde{q}(x_0,s)=1-s\tilde{S}(x_0,s)$, one gets

$$(Ł^*_{x_0}-s)\tilde{q}(x_0,s)=0, \tag{26}$$

with Dirichlet boundary condition $\tilde{q}(\pm L,s)=1$.

Finally, the moments $\langle\tau^m\rangle_{x_0}$ can be found in one of standard ways:

(i) from the moment-generating function,

$$\langle\tau^m\rangle_{x_0} = (-1)^m \lim_{s\to 0} \frac{\partial^m}{\partial s^m}\ \tilde{q}(x_0,s); \tag{27}$$

(ii) from the spectral representation of the survival probability:

$$\langle\tau^m\rangle_{x_0} = m! \sum_{n=0}^{\infty} u_n(x_0)\lambda_n^{-m} \int_{-L}^{L} dx\ u_n(x)w(x); \tag{28}$$

(iii) from recurrence partial differential equations (PDEs)

$$Ł^*_{x_0}\langle\tau^m\rangle_{x_0} = -m\langle\tau^{m-1}\rangle_{x_0}, \tag{29}$$

with Dirichlet boundary conditions [30].

In what follows, we focus on the mean exit time $\langle\tau\rangle_{x_0}$, the moment-generating function $\tilde{q}(x_0,s)$, and the survival probability $S(x_0,t)$ for harmonically trapped particles.

2.5. Mean exit time

The mean exit times of diffusive processes were studied particularly well because of their practical importance and simpler mathematical analysis (see [1, 2, 63, 64, 65] and references therein). In fact, the mean exit time,

$$\langle\tau\rangle_{x_0} = \int_0^{\infty} dt\ t\ q(x_0,t) = \int_0^{\infty} dt\ S(x_0,t), \tag{30}$$

satisfies the simpler equation than the time-dependent PDE (16):

$$Ł^*_{x_0}\langle\tau\rangle_{x_0} = -1, \tag{31}$$

with Dirichlet boundary conditions at $x_0 = \pm L$. The double integration and imposed boundary conditions yield [66]‡

$$\langle\tau\rangle_{x_0} = \frac{1}{D}\Bigg\{\Bigg[\Big(\int_{-L}^{L}\frac{dx}{w(x)}\Big)^{-1}\int_{-L}^{L}\frac{dx}{w(x)}\int_0^x dx'\ w(x')\Bigg]\int_{-L}^{x_0}\frac{dx}{w(x)} - \int_{-L}^{x_0}\frac{dx}{w(x)}\int_0^x dx'\ w(x')\Bigg\}. \tag{32}$$

Substituting $w(x)$ from Eq. (11), one gets

$$\langle\tau\rangle_{x_0} = \frac{L^2}{D}\frac{\sqrt{\pi}}{2\kappa}\Bigg\{\frac{\mathrm{erf}(i\sqrt{\kappa}(x_0/L-\varphi)) + \mathrm{erf}(i\sqrt{\kappa}(1+\varphi))}{\mathrm{erf}(i\sqrt{\kappa}(1-\varphi)) + \mathrm{erf}(i\sqrt{\kappa}(1+\varphi))} \times \int_{\sqrt{\kappa}(-1-\varphi)}^{\sqrt{\kappa}(1-\varphi)} dz\ e^{z^2}\mathrm{erf}(z) - \int_{\sqrt{\kappa}(-1-\varphi)}^{\sqrt{\kappa}(x_0/L-\varphi)} dz\ e^{z^2}\mathrm{erf}(z)\Bigg\}, \tag{33}$$

‡ In [66], the sign minus in front of $U(z)$ in the second integral in the numerator of the first term in Eq. (7.7) is missing.

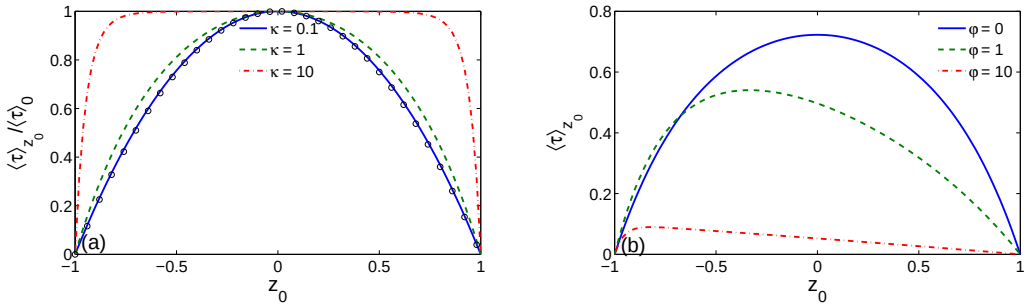

Figure 1. Mean exit time $\langle\tau\rangle_{z_0}$ as a function of $z_0 = x_0/L$: for different κ at fixed $\varphi = 0$ **(a)** and for different φ at fixed $\kappa = 1$ **(b)**. The timescale L^2/D is set to 1. For plot **(a)**, the mean exit time is divided by its maximal value (at $z_0 = 0$) in order to rescale the curves. Circles indicate the mean exit time $\frac{L^2}{2D}(1 - z_0^2)$ without trapping ($k = 0$).

where $\mathrm{erf}(z)$ is the error function, and κ and φ are two dimensionless parameters characterizing the trapping harmonic potential and the pulling constant force, respectively

$$\kappa \equiv \frac{kL^2}{2k_BT}, \qquad \varphi \equiv \frac{\hat{x}}{L} = \frac{F_0}{kL}. \tag{34}$$

Throughout the paper, we consider $\varphi \geq 0$ while all the results for $\varphi < 0$ can be obtained by replacing $\varphi \to -\varphi$ and $x_0 \to -x_0$. For large κ or φ, one can use an equivalent representation (A.1) provided in Appendix A.1.

Several limiting cases are of interest:

• When $\varphi = 0$ (i.e., $F_0 = 0$), Eq. (33) is reduced to

$$\langle\tau\rangle_{x_0} = \frac{L^2}{D}\,\frac{\sqrt{\pi}}{2\kappa}\int\limits_{\sqrt{\kappa}\ x_0/L}^{\sqrt{\kappa}} dz\ e^{z^2}\ \mathrm{erf}(z). \tag{35}$$

• In the limit $k \to 0$, one gets a simpler expression

$$\langle\tau\rangle_{x_0} = \frac{L^2}{D\eta}\left(1 - x_0/L - 2\frac{e^{-\eta x_0/L} - e^{-\eta}}{e^{\eta} - e^{-\eta}}\right), \tag{36}$$

where $\eta = F_0L/(k_BT)$ is another dimensionless parameter. If $F_0 = 0$, one retrieves the classical result for Brownian motion:

$$\langle\tau\rangle_{x_0} = \frac{L^2}{2D}\Big(1 - (x_0/L)^2\Big). \tag{37}$$

• For small κ, the Taylor expansion of Eq. (33) yields

$$\langle\tau\rangle_{x_0} \simeq \frac{L^2 - x_0^2}{2D}\left(1 + \kappa\frac{1 - 2\varphi(x_0/L) + (x_0/L)^2}{3} + O(\kappa^2)\right). \tag{38}$$

We emphasize that the limits $\kappa \to 0$ and $k \to 0$ are not equivalent because in the latter case, $\varphi \to \infty$ according to Eq. (34).

• In the opposite limit of large κ, four cases can be distinguished (see Appendix A.1):

$$\langle\tau\rangle_{x_0} \simeq \frac{L^2}{D}\begin{cases} \dfrac{\sqrt{\pi}\ e^{\kappa}}{4\kappa^{3/2}} & (\varphi = 0), \\ \dfrac{\sqrt{\pi}\ e^{\kappa(1-\varphi)^2}}{2\kappa^{3/2}(1-\varphi)} & (0 < \varphi < 1), \\ \dfrac{1}{2\kappa}\ln\dfrac{\sqrt{\kappa}(1-x_0/L)}{0.375\ldots} & (\varphi = 1), \\ \dfrac{1}{2\kappa}\ln\dfrac{\varphi - x_0/L}{\varphi - 1} & (\varphi > 1), \end{cases} \tag{39}$$

and the exponential growth in the first two relations is valid for any x_0 not too close to $\pm L$. Note that the limit of the second asymptotic relation (for $0 < \varphi < 1$) as $\varphi \to 0$ is different from the case $\varphi = 0$ by factor 2. In fact, when $\varphi > 0$, it is much more probable to reach the right endpoint than the left one, and $\langle\tau\rangle_{x_0}$ characterizes mainly the exit through the right endpoint at large κ. In turn, when $\varphi = 0$, both endpoints are equivalent that doubles the chances to exit and thus reduces by factor 2 the mean exit time. Note that the first two relations (up to a numerical prefactor) can be obtained by the Kramers theory of escape from a potential well [66, 67]. The last relation in Eqs. (39) can be retrieved from the last line of Eq. (7.9) of Ref. [66].

The behavior of the mean exit time $\langle\tau\rangle_{x_0}$ as a function of the starting point x_0 is illustrated on Fig. 1. The increase of κ at fixed $\varphi = 0$ transforms the spatial profile of the mean exit time from the parabolic shape (37) at $\kappa = 0$ to a Π-shape at large κ (Fig. 1a). In other words, the dependence on the starting point becomes weak at large κ. At the same time, the height of the profile rapidly grows with κ according to Eq. (39). On the opposite, the spatial profile becomes more skewed and sensitive to the starting point as φ increases at fixed $\kappa = 1$, while the height is decreasing (Fig. 1b). As expected, the constant force breaks the initial symmetry of the harmonic potential and facilitates the escape from the trap.

Figure 2 shows how the mean exit time $\langle\tau\rangle_0$ from the center varies with κ and φ. When there is no constant force ($\varphi = 0$), one observes a rapid (exponential) growth at large κ, in agreement with Eq. (39) (shown by circles). The presence of a moderate constant force (with $0 < \varphi < 1$) slows down the increase of the mean exit time. For instance, at $\varphi = 0.5$, $\langle\tau\rangle_0$ exhibits a broad minimum at intermediate values of κ, but it resumes growing at larger values of κ. In turn, for $\varphi \geq 1$, there is no exponential growth with κ, and the mean exit time slowly decreases, as expected from Eq. (39). Since the constant force shifts the minimum of the harmonic potential from 0 to $\hat{x} = F_0/k$, the border value $\varphi = 1$ corresponds to the minimum $\hat{x}$ at the exit position ($\hat{x} = L$). For $\varphi < 1$, the harmonic potential keeps the particle away from the exit and thus greatly increases the mean exit time. In turn, for $\varphi > 1$, the harmonic potential attracts the particle to $\hat{x}$ which is outside the interval $[-L, L]$ and thus speeds up the escape.

Although we considered the FET from a symmetric interval $[-L, L]$ for convenience, shifting the coordinate by $\hat{x}$ allows one to map the original problem to the FET from a

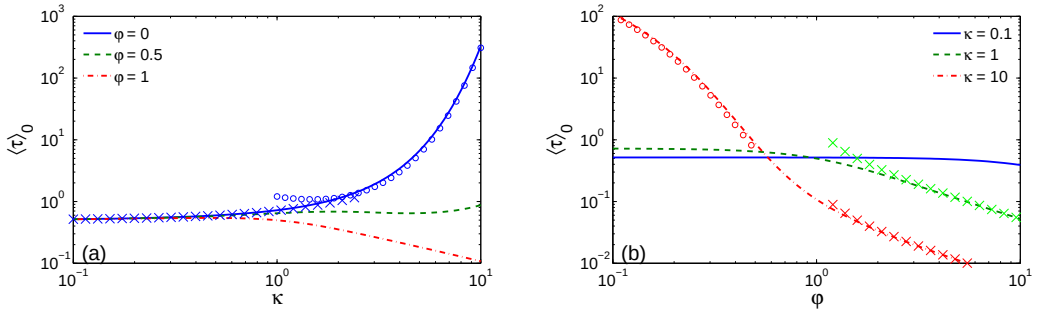

Figure 2. Mean exit time $\langle\tau\rangle_0$ as a function of κ for fixed φ **(a)** and as a function of φ for fixed κ **(b)**. The timescale L^2/D is set to 1. On both plots, circles show the exponential asymptotic relation in Eq. (39) for large κ and $0 \leq \varphi < 1$. On plot **(a)**, crosses present the asymptotic Eq. (38) for small κ, to which the next-order term, $2\kappa^2/45$, is added. On plot **(b)**, crosses present the logarithmic asymptotic relation in Eq. (39) for $\varphi > 1$.

nonsymmetric interval $[-a, b]$ with $a = L(1+\varphi)$ and $b = L(1-\varphi)$, with the starting point x_0 being shifted by $L\varphi$ to vary from $-a$ to b. As a consequence, the choice of the symmetric interval $[-L, L]$ is not restrictive, and all the results can be recast for a general interval $[-a, b]$ by shifts.

2.6. Survival probability

The survival probability is fully determined by the eigenvalues and eigenfunctions of the backward FP operator. The eigenvalue equation (13) reads

$$Du'' - (k/\gamma)(x - \hat{x})u' + \lambda u = 0. \tag{40}$$

A general solution of this equation is well known [68]

$$u(z) = c_1 M\left(-\frac{\alpha^2}{4\kappa}, \frac{1}{2}, \kappa(z-\varphi)^2\right) + c_2(z-\varphi)M\left(-\frac{\alpha^2}{4\kappa} + \frac{1}{2}, \frac{3}{2}, \kappa(z-\varphi)^2\right), \tag{41}$$

where $z = x/L$ is the dimensionless coordinate, $\lambda = D\alpha^2/L^2$, c_1 and c_2 are arbitrary constants, and

$$M(a, b, z) = {}_1F_1(a, b, z) = \sum_{n=0}^{\infty} \frac{a^{(n)} z^n}{b^{(n)} n!} \tag{42}$$

is the confluent hypergeometric function of the first kind (also known as Kummer function), with $a^{(0)} = 1$ and $a^{(n)} = a(a+1)\ldots(a+n-1) = \frac{\Gamma(a+n)}{\Gamma(a)}$, where $\Gamma(z)$ is the gamma function. The first and second terms in Eq. (41) are respectively symmetric and antisymmetric functions with respect to φ.

To shorten notations, we set

$$m^{(1)}_{\alpha,\kappa}(z) \equiv M\left(-\frac{\alpha^2}{4\kappa}, \frac{1}{2}, \kappa z^2\right), \tag{43}$$

$$m^{(2)}_{\alpha,\kappa}(z) \equiv zM\left(-\frac{\alpha^2}{4\kappa} + \frac{1}{2}, \frac{3}{2}, \kappa z^2\right), \tag{44}$$

so that

$$u(z) = c_1 m^{(1)}_{\alpha,\kappa}(z-\varphi) + c_2 m^{(2)}_{\alpha,\kappa}(z-\varphi). \tag{45}$$

The Dirichlet boundary conditions read

$$\begin{aligned} c_1 m^{(1)}_{\alpha,\kappa}(-1-\varphi) + c_2 m^{(2)}_{\alpha,\kappa}(-1-\varphi) &= 0 \qquad (\text{at } x_0 = -L), \\ c_1 m^{(1)}_{\alpha,\kappa}(1-\varphi) + c_2 m^{(2)}_{\alpha,\kappa}(1-\varphi) &= 0 \qquad (\text{at } x_0 = L). \end{aligned}$$

In the special case $\varphi = 1$, one gets $c_1 = 0$, and the eigenvalues are determined from the equation $m^{(2)}_{\alpha,\kappa}(2) = 0$. In general, for $\varphi \neq 1$, one considers the determinant of the underlying 2×2 matrix:

$$\mathcal{D}_{\alpha,\kappa,\varphi} = m^{(1)}_{\alpha,\kappa}(-1-\varphi)\; m^{(2)}_{\alpha,\kappa}(1-\varphi) - m^{(2)}_{\alpha,\kappa}(-1-\varphi)\; m^{(1)}_{\alpha,\kappa}(1-\varphi). \tag{46}$$

Setting this determinant to 0 yields the equation on α:

$$\mathcal{D}_{\alpha_n,\kappa,\varphi} = 0, \tag{47}$$

where α_n ($n = 0, 1, 2, \ldots$) denote all positive solutions of this equation (for fixed κ and φ). The eigenfunctions read then

$$u_n(z) = \frac{\beta_n}{\sqrt{L}} \Big[c^{(1)}_n m^{(1)}_{\alpha_n,\kappa}(z-\varphi) - c^{(2)}_n m^{(2)}_{\alpha_n,\kappa}(z-\varphi) \Big], \tag{48}$$

where

$$c^{(1)}_n = m^{(2)}_{\alpha_n,\kappa}(1-\varphi), \qquad c^{(2)}_n = m^{(1)}_{\alpha_n,\kappa}(1-\varphi), \tag{49}$$

and the normalization constant is

$$\beta_n^{-2} = \int_{-1-\varphi}^{1-\varphi} dz\; e^{-\kappa z^2} \Big[c^{(1)}_n m^{(1)}_{\alpha_n,\kappa}(z) - c^{(2)}_n m^{(2)}_{\alpha_n,\kappa}(z) \Big]^2. \tag{50}$$

Multiplying Eq. (40) by $w(x)$ and integrating from a to b, one gets

$$\int_a^b dx\; u(x)\; w(x) = \frac{D}{\lambda} [u'(a)w(a) - u'(b)w(b)]. \tag{51}$$

The derivative of the Kummer function can be expressed through Kummer functions, in particular,

$$\partial_z m^{(1)}_{\alpha,\kappa}(z) = \frac{\alpha^2}{2\kappa z} \Big(m^{(1)}_{\alpha,\kappa}(z) - m^{(1)}_{\sqrt{\alpha^2-4\kappa},\kappa}(z) \Big), \tag{52}$$

$$\partial_z m^{(2)}_{\alpha,\kappa}(z) = \left(2\kappa z^2 - 1 - \frac{\alpha^2}{2\kappa} \right) m^{(2)}_{\alpha,\kappa}(z) + \left(2 + \frac{\alpha^2}{2\kappa} \right) m^{(2)}_{\sqrt{\alpha^2+4\kappa},\kappa}(z), \tag{53}$$

from which one gets explicit formulas for $u_n'(a)$ and $u_n'(b)$ and thus for the integral in Eq. (51). We get therefore

$$S(x_0,t) = \sum_{n=0}^{\infty} w_n e^{-Dt\alpha_n^2/L^2} \Big[c^{(1)}_n m^{(1)}_{\alpha_n,\kappa}(x_0/L-\varphi) - c^{(2)}_n m^{(2)}_{\alpha_n,\kappa}(x_0/L-\varphi) \Big], \tag{54}$$

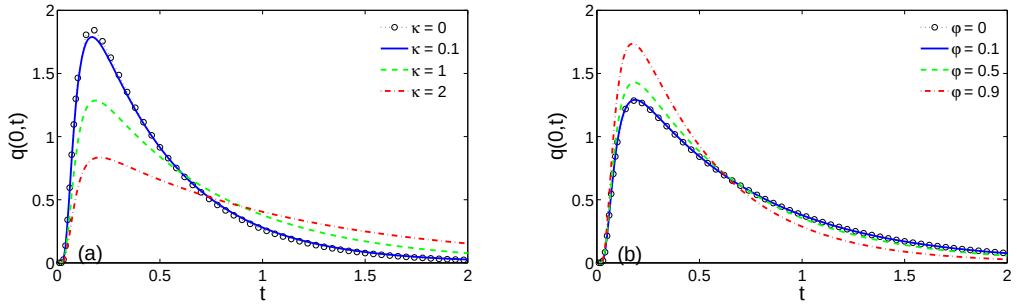

Figure 3. FET probability density $q(0,t)$ for several κ at fixed $\varphi = 0$ **(a)** and for several φ at fixed $\kappa = 1$ **(b)**. The timescale L^2/D is set to 1. The spectral decomposition (57) is truncated after 30 terms.

where

$$w_n = \frac{\beta_n^2 e^{-\kappa}}{\alpha_n^2}[v(-1) - v(1)], \tag{55}$$

with

$$v(z) = e^{2\kappa\varphi z}\Big(c_n^{(1)}\partial_z m^{(1)}_{\alpha_n,\kappa}(z-\varphi) - c_n^{(2)}\partial_z m^{(2)}_{\alpha_n,\kappa}(z-\varphi)\Big). \tag{56}$$

Taking the derivative with respect to time, one obtains the FET probability density

$$q(x_0,t) = \frac{D}{L^2}\sum_{n=0}^{\infty} w_n \alpha_n^2 e^{-Dt\alpha_n^2/L^2}\Big[c_n^{(1)} m^{(1)}_{\alpha_n,\kappa}(x_0/L-\varphi) - c_n^{(2)} m^{(2)}_{\alpha_n,\kappa}(x_0/L-\varphi)\Big]. \tag{57}$$

In the limit $\kappa \to 0$, functions $m^{(1)}_{\alpha,\kappa}(z)$ and $m^{(2)}_{\alpha,\kappa}(z)$ approach $\cos(\alpha z)$ and $\sin(\alpha z)$, respectively, so that eigenfunctions from Eq. (48) become $u_n(z) = \frac{\beta_n}{\sqrt{L}}\sin(\alpha(1-z))$, while the determinant in Eq. (46) is reduced to $\sin(2\alpha)$, from which $\alpha_n = \pi(n+1)/2$. In this limit, the dependence on φ vanishes, and one retrieves the classical result for Brownian motion

$$S(x_0,t) = 2\sum_{n=0}^{\infty}(-1)^n \frac{e^{-Dt\pi^2(n+1/2)^2/L^2}}{\pi(n+1/2)}\ \cos(\pi(n+1/2)x_0/L). \tag{58}$$

Only symmetric eigenfunctions with $\alpha_n = \pi(n+1/2)$ contribute to this expression.

For centered harmonic potential ($\varphi = 0$), Eq. (47) is reduced to

$$m^{(1)}_{\alpha_n,\kappa}(1)\ m^{(2)}_{\alpha_n,\kappa}(1) = 0, \tag{59}$$

which determines two sequences of zeros: $\alpha_{n,1}$ from $m^{(1)}_{\alpha_{n,1},\kappa}(1) = 0$, and $\alpha_{n,2}$ from $m^{(2)}_{\alpha_{n,2},\kappa}(1) = 0$. As a consequence, one can consider separately two sequences of symmetric and antisymmetric eigenfunctions: $m^{(1)}_{\alpha_{n,1},\kappa}(z)$ and $m^{(2)}_{\alpha_{n,2},\kappa}(z)$. According to Eq. (23), integration over arrival points removes all the terms containing antisymmetric eigenfunctions. This simpler situation is considered as a particular case in Sec. 2.8.

Figure 3 illustrates the behavior of the probability density $q(x_0,t)$. For fixed $\varphi = 0$, an increase of κ increases the mean exit time and makes the distribution wider. Note that the most probable FET remains almost constant. The opposite trend appears for

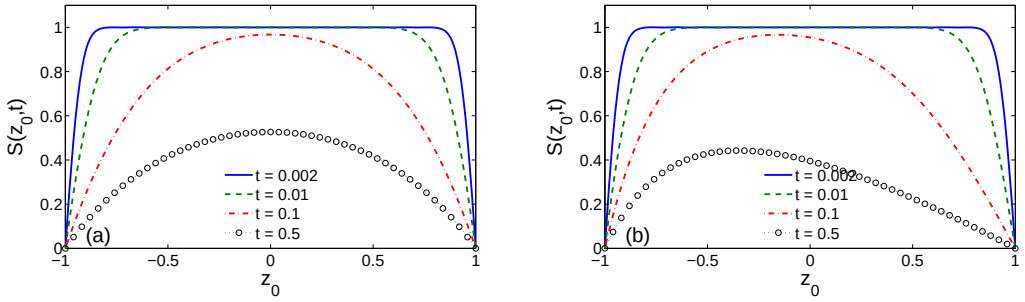

Figure 4. Survival probability $S(x_0, t)$ as a function of the starting point $z_0 = x_0/L$, with $\kappa = 1$, and $\varphi = 0$ **(a)** and $\varphi = 0.9$ **(b)**. The timescale L^2/D is set to 1. The spectral decomposition (54) is truncated after 30 terms.

variable φ at fixed $\kappa = 1$: an increase of φ diminishes the mean exit time and makes the distribution narrower. This is expected because a strong constant force would drive the particle to one exit and dominate over stochastic part.

Figure 4 shows the dependence of the survival probability $S(x_0, t)$ on the starting point x_0. At short times, the survival probability is close to 1 independently of x_0, except for close vicinity of the endpoints. As time increases, $S(x_0, t)$ is progressively attenuated. The spatial profile is symmetric for centered harmonic potential ($\varphi = 0$), and skewed to the left in the presence of a positive constant force ($\varphi = 0.9$): reaching the right endpoint is more probable due to the drift by a constant force.

2.7. Moment-generating function

Since any linear combination of functions in Eq. (45) satisfies Eq. (26), with $s = -D\alpha^2/L^2$, one can easily find the moment-generating function $\tilde{q}(x_0, s)$ by imposing the boundary condition $\tilde{q}(\pm L, s) = 1$:

$$\tilde{q}(x_0, s) = \frac{A^{(1)}_{\alpha,\kappa,\varphi}}{\mathcal{D}_{\alpha,\kappa,\varphi}} m^{(1)}_{\alpha,\kappa}(x_0/L - \varphi) + \frac{A^{(2)}_{\alpha,\kappa,\varphi}}{\mathcal{D}_{\alpha,\kappa,\varphi}} m^{(2)}_{\alpha,\kappa}(x_0/L - \varphi), \tag{60}$$

where

$$A^{(1)}_{\alpha,\kappa,\varphi} = m^{(2)}_{\alpha,\kappa}(1-\varphi) - m^{(2)}_{\alpha,\kappa}(-1-\varphi),$$
$$A^{(2)}_{\alpha,\kappa,\varphi} = m^{(1)}_{\alpha,\kappa}(-1-\varphi) - m^{(1)}_{\alpha,\kappa}(1-\varphi),$$

and $\mathcal{D}_{\alpha,\kappa,\varphi}$ is defined by Eq. (46). Setting $a = L(1+\varphi)$ and $b = L(1-\varphi)$, one retrieves the moment-generating function of the FET of an Ornstein-Uhlenbeck process from an interval $[-a, b]$ reported in [39] (p. 548, 3.0.1), in which Eq. (60) is written more compactly in terms of two-parametric family $S(\nu, a, b)$ of parabolic cylinder functions (see Appendix B.1). For symmetric interval $[-a, a]$, a similar expression for the moment-generating function was provided in [30].

It is worth noting that the probability density $q(x_0, t)$ could be alternatively found by the inverse Laplace transform of Eq. (60). For this purpose, one determines the

poles s_n of $\tilde{q}(x_0, s)$ in the complex plane which are given by zeros α_n of $\mathcal{D}_{\alpha,\kappa,\varphi}$ according to Eq. (47). In other words, one has $s_n = -D\alpha_n^2/L^2$, and the residue theorem yields

$$q(x_0,t) = \frac{4\kappa D}{L^2}\sum_{n=0}^{\infty} e^{-Dt\alpha_n^2/L^2}\Big[\frac{A^{(1)}_{\alpha_n,\kappa,\varphi}}{\mathcal{D}'_{\alpha_n,\kappa,\varphi}} m^{(1)}_{\alpha_n,\kappa}(x_0/L-\varphi) + \frac{A^{(2)}_{\alpha_n,\kappa,\varphi}}{\mathcal{D}'_{\alpha_n,\kappa,\varphi}} m^{(2)}_{\alpha_n,\kappa}(x_0/L-\varphi)\Big], \quad (61)$$

where $\mathcal{D}'_{\alpha,\kappa,\varphi}$ denotes the derivative of $\mathcal{D}_{\alpha,\kappa,\varphi}$ with respect to $s = -\alpha^2/(4\kappa)$. Comparing the above formula to Eq. (57), one gets another representation for coefficients w_n

$$w_n = \frac{4\kappa}{\alpha_n^2}\,\frac{A^{(1)}_{\alpha_n,\kappa,\varphi}}{\mathcal{D}'_{\alpha_n,\kappa,\varphi}}, \quad (62)$$

where we used the identity $c_n^{(1)} A^{(2)}_{\alpha_n,\kappa,\varphi} = -c_n^{(2)} A^{(1)}_{\alpha_n,\kappa,\varphi}$, with $c_n^{(1,2)}$ from Eq. (49). Two alternative representations (55) and (62) allow one to compute the normalization coefficients β_n without numerical integration in Eq. (50).

2.8. Higher-dimensional case

In higher dimensions, we consider the FET of a multi-dimensional Ornstein-Uhlenbeck process from a ball of radius L. For centered harmonic potential (i.e., $F_0 = 0$), the derivation follows the same steps as earlier. In fact, the integration of the probability density $p(x,t|x_0,0)$ over the arrival point x in the multi-dimensional version of Eq. (23) removes the angular dependence of the survival probability so that the eigenvalue equation is reduced to the radial part

$$\left(D\left[\partial_r^2 + \frac{d-1}{r}\partial_r\right] - \frac{kr}{\gamma}\partial_r\right) u_n(r) + \lambda_n u_n(r) = 0, \quad (63)$$

where d is the space dimension. In other words, we consider the FPT of the radial Ornstein-Uhlenbeck process to the level L. In turn, the analysis for non-centered harmonic potential with $F_0 \neq 0$ is much more involved in higher dimensions due to angular dependence, and is beyond the scope of this review.

Survival probability. A solution of Eq. (63) is given by the Kummer function which is regular at $r = 0$

$$u_n(r) = \frac{\beta_n}{L^{d/2}} M\Big(-\frac{\alpha_n^2}{4\kappa}, \frac{d}{2}, \kappa(r/L)^2\Big) \qquad (n = 0,1,2,\ldots), \quad (64)$$

where β_n is the normalization factor:

$$\beta_n^{-2} = \int_0^1 dz\; z^{d-1}\; e^{-\kappa z^2}\left[M\Big(-\frac{\alpha_n^2}{4\kappa}, \frac{d}{2}, \kappa z^2\Big)\right]^2. \quad (65)$$

The eigenvalues $\lambda_n = D\alpha_n^2/L^2$ are determined by the positive zeros α_n of the equation

$$M\Big(-\frac{\alpha_n^2}{4\kappa}, \frac{d}{2}, \kappa\Big) = 0. \quad (66)$$

Repeating the same steps as in Sec. 2.6 yields the spectral representation of the survival probability

$$S(r_0,t)=\sum_{n=0}^{\infty} w_n\ e^{-Dt\alpha_n^2/L^2} M\left(-\frac{\alpha_n^2}{4\kappa},\frac{d}{2},\kappa(r_0/L)^2\right), \tag{67}$$

where

$$w_n=\frac{\beta_n^2 e^{-\kappa}}{2\kappa}\ M\left(-\frac{\alpha_n^2}{4\kappa}+1,\frac{d}{2},\kappa\right), \tag{68}$$

and we used the identity

$$\int_0^1 dz\ z^{d-1}\ e^{-\kappa z^2}\ M\left(-\frac{\alpha_n^2}{4\kappa},\frac{d}{2},\kappa z^2\right)=\frac{e^{-\kappa}}{2\kappa}M\left(-\frac{\alpha_n^2}{4\kappa}+1,\frac{d}{2},\kappa\right). \tag{69}$$

The FET probability density is then

$$q(r_0,t)=\frac{D}{L^2}\sum_{n=0}^{\infty} w_n\ \alpha_n^2\ e^{-Dt\alpha_n^2/L^2} M\left(-\frac{\alpha_n^2}{4\kappa},\frac{d}{2},\kappa(r_0/L)^2\right). \tag{70}$$

In the limit $\kappa\to 0$, one can use the identity (see Appendix B.1)

$$\lim_{\kappa\to 0} M\left(-\frac{\alpha^2}{4\kappa},\frac{d}{2},\kappa z^2\right)=\Gamma(d/2)\frac{J_{d/2-1}(\alpha z)}{(\alpha z/2)^{d/2-1}}=\begin{cases}\cos(\alpha z) & (d=1)\\ J_0(\alpha z) & (d=2)\\ \dfrac{\sin(\alpha z)}{\alpha z} & (d=3)\end{cases} \tag{71}$$

to retrieve the classical results for Brownian motion (here $J_n(z)$ is the Bessel function of the first kind). In particular, one retrieves $\alpha_n=\pi(n+1/2)$ in one dimension and $\alpha_n=\pi(n+1)$ in three dimensions (with $n=0,1,2,\ldots$). For the one-dimensional case, we retrieved only the zeros of symmetric eigenfunctions that contribute to the survival probability (cf. discussion in Sec. 2.6).

Moment-generating function. The moment-generating function, obeying Eq. (63) with $-s$ instead of λ_n, is

$$\tilde{q}(r_0,s)=\frac{M(\frac{sL^2}{4\kappa D},\frac{d}{2},\kappa\frac{r_0^2}{L^2})}{M(\frac{sL^2}{4\kappa D},\frac{d}{2},\kappa)}, \tag{72}$$

in agreement with [39] (p. 581, 2.0.1). This function satisfies the boundary condition $\tilde{q}(L,s)=1$ and is regular at $r_0=0$. The Laplace inversion of this expression yields another representation of the probability density

$$q(r_0,t)=\frac{4\kappa D}{L^2}\sum_{n=0}^{\infty} e^{-Dt\alpha_n^2/L^2}\frac{M(-\frac{\alpha_n^2}{4\kappa},\frac{d}{2},\kappa\frac{r_0^2}{L^2})}{M'(-\frac{\alpha_n^2}{4\kappa},\frac{d}{2},\kappa)}, \tag{73}$$

where $M'(a,b,z)$ denotes the derivative of $M(a,b,z)$ with respect to a. Comparing this relation to Eq. (70), the coefficients w_n from Eq. (68) can also be identified as

$$w_n=\frac{4\kappa}{\alpha_n^2\ M'(-\frac{\alpha_n^2}{4\kappa};\frac{d}{2};\kappa)}. \tag{74}$$

As mentioned above, two expressions (68, 74) for w_n can be used to compute the normalization constants β_n without numerical integration in Eq. (65).

Mean exit time. Following the same steps as in Sec. 2.5, one gets the mean exit time for the higher-dimensional case

$$\langle\tau\rangle_{r_0} = \frac{L^2}{D}\,\frac{1}{\kappa}\int\limits_{\sqrt{\kappa}r_0/L}^{\sqrt{\kappa}} dr_1\; r_1^{1-d}e^{r_1^2}\int\limits_0^{r_1} dr_2\; r_2^{d-1}e^{-r_2^2}, \tag{75}$$

where we imposed Dirichlet boundary condition at $r_0 = L$ and the regularity condition at $r_0 = 0$. In the limit $\kappa \to 0$, one retrieves the classical result $\langle\tau\rangle_{r_0} = (L^2 - r_0^2)/(2dD)$. In the opposite limit $\kappa \gg 1$, one gets

$$\langle\tau\rangle_{r_0} \simeq \frac{L^2}{D}\,\frac{\Gamma(d/2)\; e^{\kappa}}{4\kappa^{1+d/2}} \qquad (\kappa \gg 1), \tag{76}$$

which is applicable for any r_0 not too close to L. The behavior of the mean exit time for general spherically symmetric potentials is discussed in [66].

In Appendix A.2, the asymptotic behavior of the smallest eigenvalue $\lambda_0 = D\alpha_0^2/L^2$ is obtained:

$$\lambda_0 \simeq \frac{D}{L^2}\,\frac{4\kappa^{1+d/2}}{\Gamma(d/2)}\; e^{-\kappa} \qquad (\kappa \gg 1), \tag{77}$$

which is just the inverse of the above asymptotic relation for the mean exit time. While the first eigenvalue exponentially decays with κ, the other eigenvalues linearly grow with κ (see Appendix A.2):

$$\lambda_n \simeq \frac{D}{L^2}\; 4\kappa n \qquad (\kappa \gg 1). \tag{78}$$

As a consequence, the gap between the lowest eigenvalue λ_0 and the next eigenvalue λ_1 grows linearly with κ. For $t \gg 1/\lambda_1$, the contribution of all excited eigenmodes becomes negligible as compared to the lowest mode, and the first exit time follows approximately an exponential law, $\mathbb{P}\{\tau > t\} \simeq \exp(-t/\langle\tau\rangle)$, with the mean $\langle\tau\rangle$ from Eq. (76).

We illustrate this behavior for three-dimensional case on Fig. 5a which presents the first three eigenvalues λ_n as functions of κ. Note that the correction term to the asymptotic line for λ_3 is significant even for $\kappa = 10$ (see Appendix A.2 for details). For comparison, Fig. 5b shows the first three eigenvalues for the exterior problem discussed in the next subsection.

2.9. Exterior problem

For the exterior problem, when the process is started outside the interval $[-L, L]$ (or outside the ball of radius L in higher dimensions), the FET is also referred to as the first passage time to the boundary of this domain: $\tau = \inf\{t > 0 \;:\; |X(t)| < L\}$. While the mean exit time and the probability distribution can be found in a very similar way (see below), their properties are very different from the earlier considered interior problem. For the sake of simplicity, we only consider the centered harmonic potential (i.e., $F_0 = 0$), although the noncentered case in one dimension can be treated similarly.

In one dimension, the domain $(-\infty, -L) \cup (L, \infty)$ is split into two disjoint subdomains so that τ is in fact the first passage time to a *single* barrier, either at

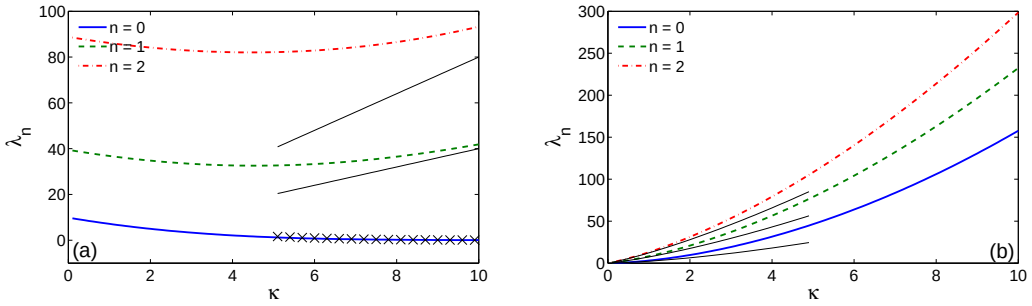

Figure 5. First three eigenvalues λ_n of the Fokker-Planck operator as functions of κ, for the interior problem **(a)** and the exterior problem **(b)** in three dimensions. The timescale L^2/D is set to 1. On plot **(a)**, crosses present the asymptotic relation (77) for the first eigenvalue λ_0 while thin solid lines indicate the asymptotic relation $4\kappa n$ for higher eigenvalues ($n = 1, 2, \ldots$). At $\kappa = 0$, one retrieves the eigenvalues $\pi^2(n+1)^2$ for Brownian motion. On plot **(b)**, thin lines indicate the asymptotic behavior (A.18) at small κ.

$x = L$ (if started from $x_0 > L$), or at $x = -L$ (if started from $x_0 < -L$). This situation is described in Appendix C.

Mean exit time. Following the steps of Sec. 2.5, one obtains the mean exit time

$$\langle\tau\rangle_{r_0} = \frac{L^2}{D}\,\frac{1}{\kappa}\int\limits_{\sqrt{\kappa}}^{\sqrt{\kappa}\,r_0/L} dr_1\; r_1^{1-d}e^{r_1^2}\int\limits_{r_1}^{\infty} dr_2\; r_2^{d-1}e^{-r_2^2}, \tag{79}$$

where we imposed Dirichlet boundary condition at $r_0 = L$ and the regularity condition at infinity.

For even dimensions d, the change of integration variables yields the explicit formula

$$\langle\tau\rangle_{r_0} = \frac{L^2}{4D\kappa}\left[2\ln(r_0/L) + \sum_{j=1}^{\frac{d}{2}-1}\frac{\Gamma(\frac{d}{2})\;\kappa^{-j}}{j\;\Gamma(\frac{d}{2}-j)}(1-(r_0/L)^{-2j})\right] \tag{80}$$

(we use the convention that $\sum_{j=1}^{n} a_n$ is zero if $n < 1$). For instance, the mean exit time in two dimensions is particularly simple:

$$\langle\tau\rangle_{r_0} = \frac{L^2}{2D\kappa}\ln(r_0/L) \qquad (d=2). \tag{81}$$

For odd d, repeated integration by parts yields

$$\langle\tau\rangle_{r_0} = \frac{L^2}{4D}\,\frac{1}{\kappa}\left\{2\sqrt{\pi}\int\limits_{\sqrt{\kappa}}^{\sqrt{\kappa}\,z_0} dz\; e^{z^2}\mathrm{erfc}(z) + \sum_{j=1}^{\frac{d-3}{2}}\left(\frac{\Gamma(\frac{d}{2})}{\Gamma(\frac{d}{2}-j)} - \frac{\Gamma(j+\frac{1}{2})}{\Gamma(\frac{1}{2})}\right)\frac{1-z_0^{-2j}}{j\;\kappa^j}\right. \tag{82}$$

$$\left. + e^{\kappa}\mathrm{erfc}(\sqrt{\kappa})\sum_{j=1}^{\frac{d-1}{2}}\Gamma\Big(\frac{d}{2}-j\Big)\kappa^{j-d/2} - e^{\kappa z_0^2}\mathrm{erfc}(\sqrt{\kappa}\;z_0)\sum_{j=1}^{\frac{d-1}{2}}\Gamma\Big(\frac{d}{2}-j\Big)(\kappa z_0^2)^{j-d/2}\right\},$$

where $z_0 = r_0/L$, and $\mathrm{erfc}(z) = 1 - \mathrm{erf}(z)$. Note that for $d = 1$, all terms vanish except the integral.

For large r_0 or large κ, the leading asymptotic term is $\frac{L^2}{2D\kappa} \ln(r_0/L)$ for all dimensions (for odd dimensions, this term comes from the integral). When r_0/L approaches 1, the mean exit time vanishes as $c(r_0/L - 1)$, where the prefactor c depends on κ and d.

When $\kappa \to 0$, the mean exit time diverges:

$$\langle \tau \rangle_{r_0} \simeq \frac{L^2}{D} \, \frac{\Gamma(\frac{d}{2})}{2(d-2)} (1 - (r_0/L)^{2-d}) \kappa^{-d/2} \quad (d \neq 2). \tag{83}$$

(for $d = 2$, see Eq. (81)). This divergence is expected because, for the exterior problem, the mean exit time for Brownian motion is infinite in all dimensions, irrespectively of its recurrent or transient character.

Finally, the mean exit time for non-centered harmonic potential (i.e., $F_0 \neq 0$) in one dimension reads for $x_0 > L$ as

$$\langle \tau \rangle_{x_0} = \frac{L^2}{D} \, \frac{\sqrt{\pi}}{2\kappa} \int_{\sqrt{\kappa}(1-\varphi)}^{\sqrt{\kappa}(x_0/L-\varphi)} dz \; e^{z^2} \; \mathrm{erfc}(z). \tag{84}$$

In the limit of large κ, two asymptotic regimes are distinguished:

(i) when $\varphi < 1$, the upper and lower limits of integration go to infinity so that the mean exit time behaves as

$$\langle \tau \rangle_{x_0} \simeq \frac{L^2}{D} \, \frac{1}{2\kappa} \ln \frac{x_0/L - \varphi}{1 - \varphi}; \tag{85}$$

(ii) when $\varphi > 1$, the lower limit of integration goes to $-\infty$, and the mean exit time exponentially diverges as

$$\langle \tau \rangle_{x_0} \simeq \frac{L^2}{D} \, \frac{\sqrt{\pi} \; e^{\kappa(\varphi-1)^2}}{2\kappa^{3/2}(\varphi - 1)}. \tag{86}$$

Both regimes are similar to that of the interior problem considered in Sec. 2.5.

Probability distribution. The moment-generating function $\tilde{q}(r_0, s)$ for the exterior problem satisfies the same equation (63), with $-s$ instead of λ_n, as $\tilde{q}(r_0, s)$ from Eq. (72) for the interior problem. In order to ensure the regularity condition at infinity (as $r_0 \to \infty$), one replaces $M(a, b, z)$ by the confluent hypergeometric function of the second kind (also known as Tricomi function):

$$U(a, b, z) = \frac{\Gamma(1-b)}{\Gamma(a-b+1)} M(a, b, z) + \frac{\Gamma(b-1)}{\Gamma(a)} \; z^{1-b} M(a-b+1, 2-b, z) \tag{87}$$

(for integer b, this relation is undefined but can be extended by continuity, see Appendix B.2). For $a > 0$, the function $U(a, b, z)$ vanishes as $z \to \infty$, in contrast to an exponential growth of $M(a, b, z)$ according to Eqs. (B.7, B.8). In turn, $U(a, b, z)$ exhibits non-analytic behavior near $z = 0$, $U(a, b, z) \simeq \frac{\Gamma(1-b)}{\Gamma(a-b+1)} + \frac{\Gamma(b-1)}{\Gamma(a)} z^{1-b} + \ldots$, that limited its use for the interior problem.

The moment-generating function for the exterior problem is then

$$\tilde{q}(r_0,s) = \frac{U(\frac{sL^2}{4\kappa D},\frac{d}{2},\kappa\frac{r_0^2}{L^2})}{U(\frac{sL^2}{4\kappa D},\frac{d}{2},\kappa)} \qquad (r_0 \geq L), \tag{88}$$

in agreement with [39] (p. 581, 2.0.1).

Denoting by α_n the positive zeros of the equation

$$U\left(-\frac{\alpha_n^2}{4\kappa},\frac{d}{2},\kappa\right) = 0, \tag{89}$$

the inverse Laplace transform yields the FET probability density:

$$q(r_0,t) = \frac{4\kappa D}{L^2}\sum_{n=0}^{\infty} e^{-Dt\alpha_n^2/L^2}\ \frac{U(-\frac{\alpha_n^2}{4\kappa},\frac{d}{2},\kappa\frac{r_0^2}{L^2})}{U'(-\frac{\alpha_n^2}{4\kappa},\frac{d}{2},\kappa)}, \tag{90}$$

where $U'(a,b,z)$ is the derivative with respect to a. Its integral over time is the survival probability:

$$S(r_0,t) = \sum_{n=0}^{\infty} w_n\ e^{-Dt\alpha_n^2/L^2}\ U\Big(-\frac{\alpha_n^2}{4\kappa},\frac{d}{2},\kappa\frac{r_0^2}{L^2}\Big), \tag{91}$$

with

$$w_n = \frac{4\kappa}{\alpha_n^2\ U'(-\frac{\alpha_n^2}{4\kappa},\frac{d}{2},\kappa)}. \tag{92}$$

Alternatively, one can use the eigenvalues $\lambda_n = D\alpha_n^2/L^2$ and the corresponding eigenfunctions

$$u_n(r) = \frac{\beta_n}{L^{d/2}}\ U\left(-\frac{\alpha_n^2}{4\kappa},\frac{d}{2},\kappa(r/L)^2\right), \tag{93}$$

where β_n is the normalization factor:

$$\beta_n^{-2} = \int_1^{\infty} dz\ z^{d-1}\ e^{-\kappa z^2}\left[U\Big(-\frac{\alpha_n^2}{4\kappa},\frac{d}{2},\kappa z^2\Big)\right]^2. \tag{94}$$

The normalization factors β_n diverge as $\kappa \to 0$.

Repeating the same steps as earlier, one retrieves the spectral representation (91) of the survival probability with

$$w_n = \frac{\beta_n^2 e^{-\kappa}}{2\kappa}\ U\left(-\frac{\alpha_n^2}{4\kappa}+1,\frac{d}{2},\kappa\right). \tag{95}$$

The asymptotic behavior of eigenvalues as $\kappa \to 0$ is discussed in Appendix A.3.

2.10. Similarities and distinctions

In spite of apparent similarities between the interior and the exterior problems, there is a significant difference in spectral properties of two problems. This difference becomes particularly clear in the limit $\kappa \to 0$ when the harmonic potential is switched off (see Fig. 5). For the interior problem, the spectrum remains discrete and continuously approaches to the spectrum of the radial Laplacian. In this limit, one retrieves the classical results

for Brownian motion (e.g., $\alpha_n \to \pi(n+1)/2$ as $\kappa \to 0$ in one dimension). In turn, the Laplace operator for the exterior problem has a continuum spectrum so that the continuous transition from discrete to continuum spectrum as $\kappa \to 0$ is prohibited. In particular, all eigenvalues λ_n vanish as $\kappa \to 0$ (see Appendix A.3). In other words, the spectral properties for infinitely small $\kappa > 0$ and $\kappa = 0$ are drastically different. One can see that the asymptotic behavior of the eigenvalues λ_n is quite different for the interior and the exterior problems.

3. Discussion

In this section, we discuss computational hints for confluent hypergeometric functions (Sec. 3.1), three applications in biophysics and finance (Sec. 3.2, 3.3, 3.4), relation to the distribution of first crossing times of a moving boundary by Brownian motion (Sec. 3.5), diffusion under quadratic double-well potential (Sec. 3.6), and further extensions (Sec. 3.7).

3.1. Computational hints

The probability distribution of first exit times involves confluent hypergeometric functions $M(a,b,z)$ (for interior problem) and $U(a,b,z)$ (for exterior problem). For instance, the eigenvalues of the Fokker-Planck operator are obtained through zeros α_n of the equation $M(-\frac{\alpha_n^2}{4\kappa}, \frac{d}{2}, \kappa) = 0$ or similar. As a consequence, one needs to compute these functions for large $|a| = \alpha_n^2/(4\kappa)$. Although the series in the definition (42) of $M(a,b,z)$ converges for all z, numerical summation becomes inaccurate for large $|a|$, and other representations of confluent hypergeometric functions are needed. In Appendix B.2, we discuss an efficient numerical scheme for rapid and accurate computation of $M(a,b,z)$ for large $|a|$ and moderate z which relies on the expansion (B.14). Moreover, we show that this scheme is as well applicable for computing the derivative of $M(a,b,z)$ with respect to a which appears in Eq. (73) or similar after the inverse Laplace transform.

For non-integer b, the Tricomi function $U(a,b,z)$ is expressed through $M(a,b,z)$ by Eq. (87) that allows one to apply the same numerical scheme for the exterior problem in odd dimensions d. Although the Tricomi function for integer b can be obtained by continuation, the derivation of its rapidly converging representation is more subtle. In practice, one can compute $U(a,b,z)$ for an integer b by extrapolation of a sequence $U(a,b_\varepsilon,z)$ computed for non-integer b_ε approaching b as $\varepsilon \to 0$.

In the case of large z and moderate $|a|$, one can use integral representations of $M(a,b,z)$ and $U(a,b,z)$ (see Appendix B.2). The same algorithms can also be applied to compute parabolic cylinder function $D_\nu(z)$ and Whittaker functions (see Appendix B.1). The Matlab code for computing both Kummer and Tricomi functions is available§

§ See `http://pmc.polytechnique.fr/pagesperso/dg/confluent/confluent.html`.

3.2. Single-particle tracking

The Langevin equation (2) can describe the thermal motion of a small tracer in a viscous medium. The Hookean force $-kX(t)$ incorporates the harmonic potential of an optical tweezer which are used to trap the tracer in a specific region of the medium [69]. Optical trapping strongly diminishes the region accessible to the tracer and thus enables to reduce the field of view and to increase the acquisition rate up to few MHz [70, 71, 72, 73, 74]. At the same time, trapping affects the intrinsic dynamics of the tracer and may screen or fully remove its features at long times. The choice of the stiffness k is therefore a compromise between risk of loosing the tracer from the field of view (too small k) and risk of suppressing important dynamical features (too large k). The FET statistics can then be used for estimating the appropriate stiffness due to a quantitative characterization of escape events. For instance, one can choose the stiffness to ensure that the mean exit time strongly exceeds the duration of experiment, or that the escape probability is below a prescribed threshold.

Another interesting option consists in detecting events in which a constant force is applied to the tracer. In living cells, such events can mimic the action of motor proteins that attach to the tracer and pull it in one direction [75, 76, 77, 78, 79]. The presence of a constant force facilitates the escape from the optical trap while higher fraction of escape events (as compared to the case without constant force) can be an indicator of such active transport mechanisms.

Originally, the idea of fast escape in the case of comparable Hookean and external forces was used to estimate the force generated by a single protein motor [75]. A "trap and escape" experiment consisted in trapping a single organelle moving along microtubules at strong stiffness and then gradually reducing it until the organelle escapes the trap. Repeating such measurement, one can estimate the "escape power" kL as a measure of the driving force F_0 when $\varphi = F_0/(kL) \sim 1$, where L is the size of the trap. In this way, the driving force generated by a single (presumably dynein-like) motor was estimated to be 2.6 pN [75]. This approximate but direct way of force measurement relies on the drastic change in the mean exit time behavior at $\varphi = 1$ according to Eq. (39).

Interestingly, these mechanisms can even be detected from a single trajectory. When there is no constant force, the mean-square displacement (MSD) of a trapped tracer, $\langle(\Delta X)^2\rangle$, is known to approach the constant level $2k_BT/k$ [52, 80, 81]. In other words, the square root of the long-time asymptotic MSD determines the typical size $\ell_k = \sqrt{2k_BT/k} = \sqrt{2D\tau_k}$ of the confining region due to optical trapping, with $\tau_k = \gamma/k$. Setting $L = q\ell_k$, one gets $\kappa = q^2$, i.e., the dimensionless parameter κ can be interpreted as the squared ratio between the exit distance L and the characteristic size of the trap ℓ_k. The above analysis showed that a tracer can rapidly reach levels which are below or slightly above ℓ_k. However, significantly longer explorations are extremely improbable. In fact, according to Eq. (76), the mean exit time for $\kappa \gg 1$ is

$$\langle\tau\rangle_0 \simeq \tau_k \, \frac{\Gamma(d/2)\, e^\kappa}{2\kappa^{d/2}} \qquad (\kappa \gg 1), \tag{96}$$

where we set $L = q\ell_k = \sqrt{\kappa}\,\sqrt{2D\tau_k}$. For large enough t (i.e., $t \gg \tau_k$), the contributions of all excited eigenstates vanish, and the survival probability exhibits a mono-exponential decay: $S(0,t) \simeq \exp(-t/\langle\tau\rangle_0)$, where we replaced the smallest eigenvalue λ_0 by $1/\langle\tau\rangle_0$ for $\kappa \gg 1$ according to Eq. (77), while $w_0 \approx 1$ as shown in Appendix A.2. In the intermediate regime $\tau_k \ll t \ll \langle\tau\rangle_0$, the survival probability remains therefore close to 1.

A constant force F_0 pulling the tracer from the optical trap strongly affects the mean exit time and the survival probability. The dimensionless parameter φ from Eq. (34) is the ratio between the new stationary position $\hat{x}$ of the trajectory and the exit level $L = \sqrt{\kappa}\,\ell_k$:

$$\varphi = \frac{F_0}{kL} = \frac{\hat{x}}{\ell_k\sqrt{\kappa}} = \frac{F_0\sqrt{2D\tau_k}}{2k_BT\sqrt{\kappa}}. \tag{97}$$

For large φ, the mean exit time can be approximated according to Eq. (39) as $\langle\tau\rangle_0 \simeq \tau_k \ln\frac{\varphi}{\varphi-1} \simeq \tau_k/\varphi$, i.e., it becomes smaller than τ_k, and much smaller than the mean exit time from Eq. (96) without force. As expected, exit events would be observed much more often in the presence of strong constant force.

For a long acquired trajectory, one can characterize how often different levels are reached. Strong deviations from the expected statistics (given by the survival probability) would suggest the presence of a constant force. To illustrate this idea, we simulate the thermal motion of a spherical tracer of radius $a = 1$ μm submerged in water and trapped by an optical tweezer with a typical stiffness constant $k = 10^{-6}$ N/m [73, 74]. The Stokes relation implies $\gamma = 6\pi a\eta_0 \approx 1.88 \cdot 10^{-8}$ kg/s, from which the diffusion coefficient is $D = k_BT/\gamma \approx 2.20 \cdot 10^{-13}$ m^2/s at $T = 300$ K (with $\eta_0 \approx 10^{-3}$ kg/m/s being the water viscosity). The characteristic trapping time is $\tau_k = \gamma/k \approx 18.8$ ms, while the confinement length is $\ell_k = \sqrt{2k_BT/k} \approx 91$ nm. Figure 6a shows one simulated trajectory of the tracer. According to Eq. (33), the mean exit times from the intervals $(-\ell_k, \ell_k)$ and $(-2\ell_k, 2\ell_k)$ are 27.2 ms and 517 ms, respectively. For a generated sample of duration 1 s, one observes multiple crossings of levels $\pm\ell_k$ and only few crossings of levels $\pm2\ell_k$. For comparison, we generated another trajectory for which a constant force $F_0 = 0.2$ pN (yielding $\varphi = 2.20/\sqrt{\kappa}$) is applied between 0.3 s and 0.5 s (Fig. 6b). Since motor proteins exert forces which are typically tenfold higher [75, 76], their effect is expected to be much stronger and thus easier to detect. The constant force reduces the mean exit times to 9.8 ms and 28 ms, i.e., by factors 2.8 and 18, respectively. As expected, once the constant force is applied, the tracer tends to reach the new stationary level $\hat{x} = 200$ nm so that the trajectory crosses the level ℓ_k and remains above this level for whole duration of the forced period. Once the force is switched off, the trajectory returns to its initial regime with zero mean. One can see that the use of FET statistics presents a promising perspective for design and analysis of single-particle tracking experiments, while Bayesian techniques can be further applied to get more reliable results [82, 83]. Note that the FPT statistics have also been suggested as robust estimators of diffusion characteristics [84] (see also [26]). Another method

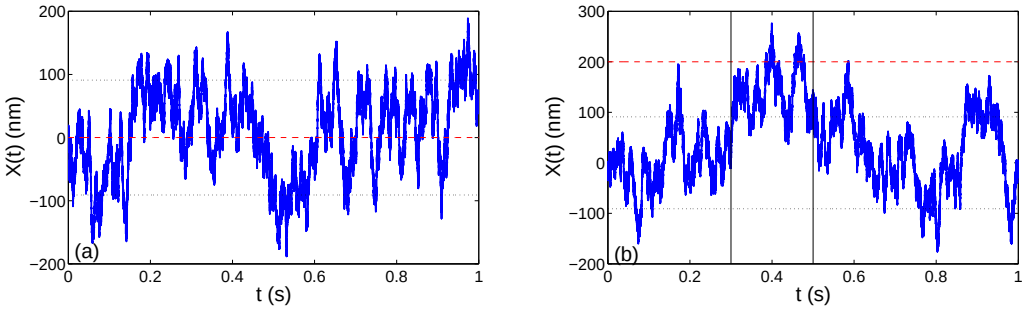

Figure 6. Two simulated trajectories of a spherical tracer submerged in water under the optical trapping: **(a)** no constant force; **(b)** constant force $F_0 = 0.2$ pN is applied between 0.3 and 0.5 s (indicated by vertical lines). Horizontal dotted lines indicate the typical trapping size $\pm\ell_k = 91$ nm, while dashed red line shows the stationary level $\hat{x}$ (equal to 0 for zero force and 200 nm for $F_0 = 0.2$ pN). The other parameters are provided in the text.

relying on the time evolution of the tracer probability distribution was proposed for simultaneously extracting the restoring-force constant and diffusion coefficient [85].

At the same time, we emphasize that this perspective needs further analysis. First, we focused on normal diffusion in a harmonic potential while numerous single-particle tracking experiments evidenced anomalous diffusion in living cells and polymer solutions [73, 86, 87, 88, 89]. Several theoretical models have been developed to describe anomalous processes such as continuous-time random walks (CTRW), fractional Brownian motion (fBm), and generalized Langevin equation [5, 6, 78, 79]. While an extension of the presented results is rather straightforward for CTRW (Sec. 3.7), the FPT problems for non-Markovian fBm or generalized Langevin equation are challenging due to lack of equivalent Fokker-Planck formulation. Second, the quadratic profile is an accurate approximation for optical trapping potential only for moderate deviations from the center of the laser beam [69], while the spatial profile can be more complicated for strong deviations. In other words, an accurate description of the tracer escape may require more sophisticated analysis. Finally, the inference of constant forces from a single trajectory may present some statistical challenges because different escape events can be correlated.

3.3. Adhesion bond dissociation under mechanical stress

We briefly mention another biophysical example of bond dissociation. Adhesion between cells or of cells to surfaces is mediated by weak noncovalent interactions. While a reversible bond between two molecules can break spontaneously (due to thermal fluctuations), an external force is needed to rupture multiple bonds that link two cells together [90]. The dynamics of bond rupture can be seen as the first exit time problem in which exit or escape occurs when the intermolecular distance exceeds an effective interaction radius. Bell suggested to apply the kinetic theory of the strength of solids

to describe the lifetime of a bond (i.e., the mean exit time) as

$$t_b = t_0 \exp[(E_b - r_b F_0)/(k_B T)], \tag{98}$$

where E_b is the bond energy, r_b is the range of the minimum of the binding free energy, F_0 is the applied external force per bond, and t_0 is the lifetime at the critical force E_b/r_b at which the minimum of the free energy vanishes [90]. This relation became a canonical description of adhesion bond dissociation under force.

If the binding potential can be approximated as quadratic, then the lifetime of a bond is precisely the mean exit time $\langle\tau\rangle$ of a harmonically trapped particle. In that case, the second asymptotic relation in Eqs. (39) implies the quadratic dependence on the force, $\langle\tau\rangle \sim e^{\kappa(1-\varphi)^2}$, where $\varphi = F_0/(kr_b)$, and $\kappa = E_b/(k_B T) = kr_b^2/(2k_B T)$. In other words, Eq. (98) is retrieved only for weak forces when the quadratic term φ^2 can be neglected. However, in the regime where the bond is most likely to break, the applied force is large, and the mean exit time may have completely different asymptotics (see, e.g., the last line of Eqs. (39) for $\varphi > 1$). This discrepancy was already outlined in Ref. [91], in which the cases of a harmonic potential and an inverse power law attraction were discussed, and in Ref. [92] which presented molecular dynamics study of unbinding and the related analysis of first exit times. Other effects such as the dependence of the bond strength and survival time on the loading rate, were investigated both theoretically and experimentally (see [91, 92, 93, 94, 95, 96] and references therein).

3.4. Algorithmic trading

Algorithmic trading is another field for applications of FETs. In algorithmic trading, a set of trading rules is developed in order to anticipate the next price variation of an asset from its earlier (historical) prices [97]. Although the next price is random (and thus unpredictable), one aims to catch some global or local trends which can be induced by collective behavior of multiple traders or macroeconomic tendences [98, 99, 100]. Many trading strategies rely on the exponential moving average $\bar{p}_n$ of the earlier prices p_k [101, 102, 103, 104]

$$\bar{p}_n = \lambda \sum_{k=0}^{\infty} (1-\lambda)^k p_{n-k}, \tag{99}$$

where $0 < \lambda \leq 1$ characterizes how fast the exponential weights of more distant prices decay. The difference between the current price p_n and the "anticipated" average price $\bar{p}_n$,

$$\delta_n \equiv p_n - \bar{p}_n = (1-\lambda) \sum_{k=0}^{\infty} (1-\lambda)^k r_{n-k}, \qquad (r_n = p_n - p_{n-1}), \tag{100}$$

can be seen as an indicator of a new trend. For independent Gaussian price variations r_n, writing $\delta_{n+1} = (1-\lambda)\delta_n + (1-\lambda)r_{n+1}$, one retrieves Eq. (6) for a discrete version of an Ornstein-Uhlenbeck process, where $\hat{x} = \mu(1-\lambda)/\lambda$ is related to the mean price

variation μ, $\theta = -\ln(1-\lambda)$, and $\sigma = \sigma_0 \frac{(1-\lambda)\sqrt{2\theta}}{\sqrt{1-(1-\lambda)^2}}$ is proportional to the standard deviation (volatility) σ_0 of price variations.

The indicator δ_n can be used in both mean-reverting and trend following strategies. In the mean-reverting frame, if δ_n exceeds a prescribed threshold L, this is a trigger to sell the asset at its actual (high) price, in anticipation of its return to the expected (lower) level $\bar{p}_n$ in near future. Similarly, the event $\delta_n < -L$ triggers buying the asset. In the opposite trend following frame, the condition $\delta_n > L$ is interpreted as the beginning of a strong trend and thus the signal to buy the asset at its actual price, in anticipation of its further growth (similarly for $\delta_n < -L$). In other words, the same condition $\delta_n > L$ (or $\delta_n < -L$) can be interpreted differently depending on the empirical knowledge on the asset behavior. Whatever the strategy is used, the statistics of crossing of the prescribed levels $\pm L$ is precisely the FET problem. Theoretical results in Sec. 2 can help to characterize durations between buying and selling moments. In particular, the choice of the threshold L is a compromise between execution of too frequent buying/selling transactions (i.e., higher transaction costs) at small L and missing intermediate trends (i.e. smaller profits) at large L. We also note that Ornstein-Uhlenbeck processes often appear in finance to model, e.g., interest rates (Vasicek model) and currency exchange rates [105, 106]. A general frame of using eigenfunctions for pricing options is discussed in [107].

3.5. First crossing of a moving boundary by Brownian motion

The first exit time problem can be extended to time-evolving domains [108, 109, 110, 111, 112]. For instance, one can investigate the first passage time of Brownian motion to a time-dependent barrier $L(t)$, $\tau = \inf\{t > 0 \ : \ X(t) = L(t)\}$, or the first exit time from a symmetric "envelope" $[-L(t), L(t)]$, $\tau = \inf\{t > 0 \ : \ |X(t)| = L(t)\}$. Although the survival probability $S(x_0, t)$ satisfies the standard diffusion equation with Dirichlet boundary condition, the boundary $L(t)$ evolves with time. For a smooth $L(t)$, setting $S(x_0, t) = v(z, t)$ with a new space variable $z = x_0/L(t)$ yields

$$\frac{\partial v(z,t)}{\partial t} = \frac{D}{L(t)^2}\, \partial_z^2 v(z,t) - \frac{L'(t)}{L(t)}\, z\, \partial_z v(z,t), \tag{101}$$

with Dirichlet boundary condition $v(\pm 1, t) = 0$ at two *fixed* endpoints (here we focus on the exit time). Setting a new time variable $T = \ln(L(t)/L(0))$, the above equation can also be written as the backward Fokker-Planck equation with time-dependent diffusion coefficient $D(T) = D\frac{1}{L'(t)L(t)} = D\frac{e^{-T}}{L(0)\ L'(L^{-1}(L(0)e^T))}$ and a centered harmonic potential:

$$\frac{\partial v(z,T)}{\partial T} = D(T)\partial_z^2 v(z,T) - z\, \partial_z v(z,T). \tag{102}$$

In higher dimensions, the second derivative ∂_z^2 is simply replaced by the radial Laplace operator $\partial_r^2 + \frac{d-1}{r}\partial_r$.

In general, the above equation does not admit explicit solutions. A notable exception is the case of square-root boundaries which has been thoroughly investigated

[113, 114, 115, 116, 117, 118]. In fact, when $L(t) = \sqrt{2b(t+t_0)}$ (with $b > 0$ and $t_0 > 0$), one has $L'(t)L(t) = b$ so that $D(T)$ is independent of T (or t). In other words, one retrieves the backward Fokker-Planck problem (17, 24) with $\hat{x} = 0$, $k/\gamma = 1$, $L = 1$, and D replaced by D/b. Its exact solution is given by Eq. (73) for d-dimensional case:

$$q(z_0, T) = 2\sum_{n=0}^{\infty} e^{-2T\nu_n} \frac{M(-\nu_n, \frac{d}{2}, \frac{bz_0^2}{2D})}{M'(-\nu_n, \frac{d}{2}, \frac{b}{2D})}, \tag{103}$$

where $z_0 = r_0/L(0) = r_0/\sqrt{2bt_0}$ denotes the rescaled starting point r_0, and $\nu_n = \alpha_n^2/(4\kappa)$ are zeros of $M(-\nu, \frac{d}{2}, \frac{b}{2D}) = 0$. Changing back T to t, one gets

$$p(z_0, t) = \frac{1}{t_0}\sum_{n=0}^{\infty}(1 + t/t_0)^{-\nu_n - 1} \frac{M(-\nu_n, \frac{d}{2}, \frac{bz_0^2}{2D})}{M'(-\nu_n, \frac{d}{2}, \frac{b}{2D})}, \tag{104}$$

This expression in a slightly different form was provided for $d = 1$ in [118]. Note also that the probability $\mathbb{P}\{\sup_{1<t<T}(|W_t|/\sqrt{t}) < c\}$ admits a similar expansion [119].

In addition, Eq. (72) yields

$$t_0^{-\nu}\langle(\tau + t_0)^\nu\rangle = \langle e^{2\nu T}\rangle = \tilde{q}(z_0, -2\nu) = \frac{M(-\nu, \frac{d}{2}, \frac{bz_0^2}{2D})}{M(-\nu, \frac{d}{2}, \frac{b}{2D})}, \tag{105}$$

from which one retrieves

$$\langle(\tau + t_0)^\nu\rangle = \frac{t_0^\nu}{M(-\nu, \frac{d}{2}, \frac{b}{2D})} \qquad (\text{at } z_0 = 0), \tag{106}$$

that was reported for $d = 1$ in [114]. Note that the ν-th moment exists under the condition $\Re\{\nu\} < \nu_0$, as clearly seen from Eq. (104). In the special case $b = D$, the square-root boundary $L(t) = \sqrt{2b(t+t_0)}$ grows in the same way as the root-mean-square of Brownian motion $\sqrt{\langle W_t^2\rangle} = \sqrt{2Dt}$. Since $\nu_0 = 1$ at $b = D$, the mean exit time is infinite. More generally, the mean exit time is infinite for broader envelopes ($b \geq D$) and finite for narrower envelopes ($b < D$), as expected. The shift t_0 plays a minor role of a time scale.

3.6. Quadratic double-well potential

The above spectral approach can be extended to more complicated trapping potentials. As an example, we briefly describe diffusion under double-well (or bistable) piecewise quadratic potential:

$$V(x) = \begin{cases} \dfrac{1}{2}k_1(x + x_1)^2, & x \leq 0, \\ \dfrac{1}{2}k_2(x - x_2)^2 + v_0, & x \geq 0, \end{cases} \tag{107}$$

where two minima are located at $-x_1$ and x_2 (with $x_1 > 0$ and $x_2 > 0$), k_1 and k_2 are two spring constants, and $v_0 = \frac{1}{2}(k_1x_1^2 - k_2x_2^2)$ is a constant ensuring the continuity of the potential at $x = 0$. The resulting Langevin equation remains linear, in contrast to other bistable potentials such as a quartic potential (e.g., $V(x) = ax^4 + bx^2 + cx$). The diffusive dynamics under double-well potentials was thoroughly investigated by

using general theoretical tools (e.g. Kramers' theory [66, 67] or WKB approximation [120, 121, 122]) and exactly solvable models (see [123, 124, 125, 126, 127, 128, 129] and references therein).

For each semi-axis, an eigenfunction satisfies Eq. (40) with the proper k_i. However, neither Kummer, nor Tricomi function is appropriate to represent the solution in this case. In fact, the Kummer function $M(a, 1/2, z^2)$ rapidly grows at infinity, while the Tricomi function $U(a, 1/2, z^2)$ behaves as $\frac{\sqrt{\pi}}{\Gamma(a+1/2)} - \frac{2\sqrt{\pi}}{\Gamma(a)}|z| + \ldots$ for small z, i.e., its derivative is discontinuous at 0. A convenient representation can still be obtained as a linear combination of two Kummer functions, in which the rapid growth of these functions is compensated. This is precisely the case of parabolic cylinder functions $D_\nu(z)$ and $D_\nu(-z)$ which vanish as $z \to \infty$ (resp., $z \to -\infty$) but rapidly grow as $z \to -\infty$ (resp. $z \to \infty$) unless ν is a nonnegative integer [see Eqs. (B.3), (D.2), (D.3)]. An eigenfunction can therefore be written as

$$u(x) = \begin{cases} c_1 e^{\kappa_1 (x/x_1+1)^2/2} D_{\nu_1}\Big(-\sqrt{2\kappa_1}(x/x_1+1)\Big), & x \le 0, \\ c_2 e^{\kappa_2 (x/x_2-1)^2/2} D_{\nu_2}\Big(\sqrt{2\kappa_2}(x/x_2-1)\Big), & x \ge 0, \end{cases} \tag{108}$$

where $\kappa_i = k_i x_i^2/(2k_BT)$, $\nu_i = \lambda x_i^2/(2\kappa_i D)$, and λ, c_1, c_2 are determined by normalization and two interface conditions at $x = 0$. The continuity of the eigenfunction at $x = 0$ can be satisfied by choosing

$$c_1 = \beta\ e^{\kappa_2/2} D_{\nu_2}(-\sqrt{2\kappa_2}), \qquad c_2 = \beta\ e^{\kappa_1/2} D_{\nu_1}(-\sqrt{2\kappa_1}),$$

where β is a normalization constant.

The second interface condition is deduced from the orthogonality of eigenfunctions with two weights $w_{1,2}$ from Eq. (11) for positive and negative semi-axes,

$$w_i(x) = \exp(\kappa_i[1 - (x/x_i \pm 1)^2]),$$

where plus (resp., minus) corresponds to $i = 1$ (resp., $i = 2$). The orthogonality imposes the interface condition

$$D w_1(0) u'(0^-) - D w_2(0) u'(0^+) = 0, \tag{109}$$

where the same diffusion coefficient D is assumed on both sides. Since $w_i(0) = 1$, one retrieves the standard flux continuity equation, $u'(0^-) = u'(0^+)$, yielding an equation determining the eigenvalues λ:

$$\begin{aligned} &x_1 D_{\nu_1}(-\sqrt{2\kappa_1})\Big[2\kappa_2 D_{\nu_2}(-\sqrt{2\kappa_2}) + \sqrt{2\kappa_2} D_{\nu_2+1}(-\sqrt{2\kappa_2})\Big] + \\ &x_2 D_{\nu_2}(-\sqrt{2\kappa_2})\Big[2\kappa_1 D_{\nu_1}(-\sqrt{2\kappa_1}) + \sqrt{2\kappa_1} D_{\nu_1+1}(-\sqrt{2\kappa_1})\Big] = 0, \end{aligned}$$

where we used the identity $\frac{\partial}{\partial z} D_\nu(z) = \frac{z}{2} D_\nu(z) - D_{\nu+1}(z)$, and λ appears in $\nu_i = \lambda x_i^2/(2\kappa_i D)$. The smallest eigenvalue $\lambda = 0$ corresponds to the steady state.

The normalization constant β is found according to

$$\beta^{-2} = e^{\kappa_1+\kappa_2} \left[\frac{x_1 D_{\nu_2}^2(-\sqrt{2\kappa_2})}{\sqrt{2\kappa_1}} \int\limits_{-\sqrt{2\kappa_1}}^{\infty} dz\ D_{\nu_1}^2(z) + \frac{x_2 D_{\nu_1}^2(-\sqrt{2\kappa_1})}{\sqrt{2\kappa_2}} \int\limits_{-\sqrt{2\kappa_2}}^{\infty} dz\ D_{\nu_2}^2(z) \right], \tag{110}$$

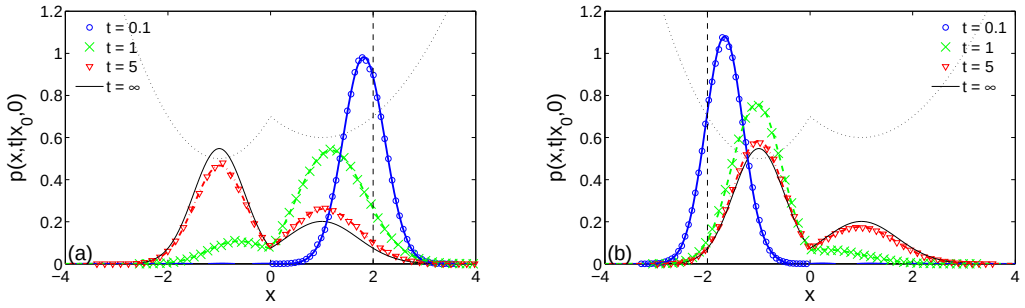

Figure 7. Evolution of the probability density $p(x,t|x_0,t_0)$ for diffusion under quadratic double-well potential (sketched by black dotted line) with two minima at ± 1 (i.e. $x_1 = x_2 = 1$), and $\kappa_1 = 2$, $\kappa_2 = 1$. Dashed vertical line indicates the starting point at $t_0 = 0$: $x_0 = 2$ **(a)** and $x_0 = -2$ **(b)**. Symbols represent normalized histograms of arrival positions obtained by Monte Carlo simulations of an adapted version of Eq. (6) (with time step $\delta = 10^{-3}$ and 10^5 sample trajectories), while lines show the spectral decomposition (18) with 50 terms. We set $D = 1$.

in which both integrals can be partly computed by using the identity [130]

$$\int_0^\infty dz\ D_\nu^2(z) = \frac{\sqrt{\pi}}{2^{3/2}}\ \frac{\psi(\frac{1-\nu}{2}) - \psi(-\frac{\nu}{2})}{\Gamma(-\nu)}, \tag{111}$$

where $\psi(z) = \Gamma'(z)/\Gamma(z)$ is the digamma function. The lowest eigenfunction corresponding to $\lambda_0 = 0$, is constant, $u_0(x) = \beta_0$, with

$$\beta_0^{-2} = \frac{\sqrt{\pi}}{2}\left[\frac{x_1 e^{\kappa_1}(1+\mathrm{erf}(\sqrt{\kappa_1}))}{\sqrt{\kappa_1}} + \frac{x_2 e^{\kappa_2}(1+\mathrm{erf}(\sqrt{\kappa_2}))}{\sqrt{\kappa_2}}\right].$$

As a consequence, one retrieves the equilibrium Boltzmann-Gibbs distribution, $p_{\rm eq}(x) = p(x,\infty|x_0,0) = u_0(x_0)u_0(x)w(x) = \beta_0^2 w(x)$.

Figure 7 illustrates the evolution of the probability density $p(x,t|x_0,t_0)$ for diffusion under quadratic double-well potential with two minima at ± 1 (i.e., $x_1 = x_2 = 1$) and two different dimensionless strengths: $\kappa_1 = 2$ and $\kappa_2 = 1$. One can see how the initial Dirac distribution, concentrated at $x_0 = 2$ (Fig. 7a) or $x_0 = -2$ (Fig. 7b) and shown by dashed vertical line, is progressively transformed into the equilibrium distribution $p_{\rm eq}(x)$ (shown by black solid line). Other diffusion characteristics can be deduced from the probability density.

3.7. Further extensions

The spectral approach is a general tool for computing FETs and other first-passage quantities. We briefly mention four straightforward extensions.

(i) In one dimension, one can easily derive the splitting probability $H(x_0)$, i.e., the probability to exit from one endpoint (e.g., $x_0 = L$) before the other ($x_0 = -L$). The splitting probability is governed by the stationary equation $\text{Ł}^*_{x_0} H(x_0) = 0$ so that $H(x_0)$

is given by a general solution in Eq. (45) with $\alpha = 0$. Two constants c_1 and c_2 are set by boundary conditions $H(L) = 1$ and $H(-L) = 0$, from which

$$H(x_0) = \frac{\mathrm{erf}(i\sqrt{\kappa}(x_0/L - \varphi)) + \mathrm{erf}(i\sqrt{\kappa}(1+\varphi))}{\mathrm{erf}(i\sqrt{\kappa}(1-\varphi)) + \mathrm{erf}(i\sqrt{\kappa}(1+\varphi))}, \tag{112}$$

where we used $M(0, b, z) = 1$ and $M(1/2, 3/2, z) = \frac{\sqrt{\pi}\ \mathrm{erf}(i\sqrt{z})}{2i\sqrt{z}}$. Note that this expression can be recognized in Eq. (33) for the mean exit time.

(ii) Dirichlet boundary conditions, $q(\pm L, t) = 0$, were imposed on the FET probability density at both endpoints in order to stop the process whenever it exits from the interval. One can consider other boundary value problems, e.g., with one reflecting endpoint or one/two semi-reflecting points. In this case, Dirichlet boundary condition at one or both endpoints is replaced by Neumann or Robin boundary conditions [46]. For instance, the condition $\frac{\partial}{\partial x_0} q(x_0, t) = 0$ at $x_0 = -L$ describes the reflecting barrier at $-L$. The Robin boundary condition, $\frac{\partial}{\partial x_0} q(x_0, t) + hq(x_0, t) = 0$, allows one to consider partial absorptions/reflections for modeling various transport mechanisms on the boundary and to switch continuously between Neumann (pure reflections) and Dirichlet (pure absorptions) cases by varying h from 0 to infinity [131, 132, 133, 134, 135, 136, 137]. The solution can be obtained in the same way.

(iii) The first passage time to a single barrier can be deduced from the first exit time from an interval by sending one endpoint to infinity (see Appendix C).

(iv) A straightforward extension of the spectral approach allows one to deduce FETs of continuous-time random walks (CTRW) [5, 6]. In this model, long stalling periods between moves result in anomalous subdiffusion, when the mean-square displacement evolves sublinearly with time: $\langle (X(t) - X(0))^2 \rangle \simeq 2D_\alpha t^\alpha$, with the exponent $0 < \alpha < 1$ and the generalized diffusion coefficient D_α. The same derivations can be formally repeated for the fractional Fokker-Planck equation that governs the survival probability of CTRWs. In practice, it is sufficient to replace s/D by s^α/D_α in the Laplace domain that in time domain yields the replacement of exponential functions $\exp(-\lambda_n t)$ by Mittag-Leffler functions $E_\alpha(-\lambda_n D_\alpha t^\alpha/D)$ in spectral decompositions such as Eq. (23) or similar. As expected for CTRWs, the mean exit time diverges due to long stalling periods while the survival probability exhibits a power law decay $t^{-\alpha}$ at long times instead of the exponential decay for normal diffusion.

Conclusion

We revised the classical problem of finding first exit times for harmonically trapped particles. Although the explicit formulas for the moment-generating function $\langle e^{-s\tau} \rangle$ can be found in standard textbooks (e.g., [39]), the computation of the probability density and the survival probability through the inverse Laplace transform requires substantial analysis of confluent hypergeometric functions. For didactic purpose, we reproduced the main derivation steps and resulting spectral decompositions that involve the eigenvalues and eigenfunctions of the governing Fokker-Planck operator. We also provided explicit

formulas for the mean exit time and discussed its asymptotic behavior in different limits. We considered the general case of non-centered harmonic potential in one dimension (Ornstein-Uhlenbeck process with nonzero mean) and the centered harmonic potential in higher dimensions (radial Ornstein-Uhlenbeck process). Both interior and exterior problems were analyzed.

After revising this classical problem, we discussed some practical issues. First, we described a rapidly converging series representation of confluent hypergeometric functions which is particularly well suited for rapid numerical computation of eigenvalues and eigenfunctions of the governing Fokker-Planck operator. Second, we showed how the mean exit time and the survival probability can be used for the analysis of single-particle tracking experiments with optically trapped tracers. The derived formulas allow one to choose the appropriate value of the optical tweezers' stiffness and to detect in acquired trajectories the active periods with nonzero force exerted by motor proteins. Third, we mentioned the relation of the first exit time problem to the dynamics of bond dissociation under mechanical stress which plays an important role in cell adhesion and motility. Fourth, we considered an application of FETs for algorithmic trading in stock markets in which buying or selling signals are triggered when the difference between the current and anticipated prices exceeds a prescribed threshold. In a first approximation, these events correspond to exits of an Ornstein-Uhlenbeck process from an interval so that the FET statistics can be used to estimate strategy holding periods and to choose the appropriate threshold that ensures the desired transaction rate. Fourth, we mentioned the relation to the distribution of first crossing times of a moving boundary by Brownian motion. Finally, we discussed several extensions of the spectral approach, including diffusion under quadratic double-well potential and anomalous diffusion.

Acknowledgments

The author acknowledges partial support by the grant ANR-13-JSV5-0006-01 of the French National Research Agency.

Appendix A. Limit of large κ

Appendix A.1. Mean exit time

For large κ or φ, Eq. (33) is not appropriate for numerical computation of the mean exit time because integrals and error functions are exponentially large. Re-arranging these terms, one can rewrite Eq. (33) as

$$\langle\tau\rangle_{z_0} = \frac{L^2}{D}\frac{\sqrt{\pi}}{2\kappa}\left\{\frac{1+e^{-2\kappa\varphi(1+z_0)-\kappa(1-z_0^2)}\frac{D(\sqrt{\kappa}(z_0-\varphi))}{D(\sqrt{\kappa}(1+\varphi))}}{1+e^{-4\kappa\varphi}\frac{D(\sqrt{\kappa}(1-\varphi))}{D(\sqrt{\kappa}(1+\varphi))}}\right. \tag{A.1}$$
$$\left.\times\int\limits_{\sqrt{\kappa}(\varphi-1)}^{\sqrt{\kappa}(1+\varphi)} dz\; e^{z^2}\mathrm{erfc}(z) - \int\limits_{\sqrt{\kappa}(\varphi-z_0)}^{\sqrt{\kappa}(1+\varphi)} dz\; e^{z^2}\mathrm{erfc}(z)\right\},$$

where $z_0 = x_0/L$, and $D(x)$ is the Dawson function:

$$D(x) = e^{-x^2} \int_0^x dt\ e^{t^2}, \tag{A.2}$$

which is related to the error function of imaginary argument as

$$\mathrm{erf}(ix) = \frac{2i}{\sqrt{\pi}} e^{x^2} D(x). \tag{A.3}$$

For large x, the Dawson function decays as

$$D(x) \simeq \frac{1}{2x} + \frac{1}{4x^3} + \frac{3}{8x^5} + \ldots. \tag{A.4}$$

The relation (A.1) allows one to compute the mean exit time in the limit of large κ and/or φ. In fact, since the Dawson function vanishes for large argument, the ratio in front of the first integral in Eq. (A.1) becomes exponentially close to 1 so that

$$\langle \tau \rangle_{z_0} \simeq \frac{L^2}{D} \frac{\sqrt{\pi}}{2\kappa} \int_{\sqrt{\kappa}(\varphi-1)}^{\sqrt{\kappa}(\varphi-z_0)} dz\ e^{z^2} \mathrm{erfc}(z). \tag{A.5}$$

Three situations can be considered separately.

(i) If $\varphi > 1$, the upper and lower limits of the above integral are positive and large so that

$$\langle \tau \rangle_{z_0} \simeq \frac{L^2}{D}\ \frac{1}{2\kappa} \ln \frac{\varphi - z_0}{\varphi - 1} \qquad (\kappa \gg 1), \tag{A.6}$$

where we used the asymptotic relation

$$\int_a^b dz\ e^{z^2} \mathrm{erfc}(z) \simeq \frac{\ln(b/a)}{\sqrt{\pi}} \qquad (a, b \gg 1). \tag{A.7}$$

Note that Eq. (A.6) is accurate already for $\varphi \gtrsim 2$ (and $\kappa \geq 1$).

(ii) If $0 < \varphi < 1$ but $\kappa \to \infty$, the lower limit goes to $-\infty$, and the integral exponentially diverges:

$$\langle \tau \rangle_0 \simeq \frac{L^2}{D}\ \frac{\sqrt{\pi}\ e^{\kappa(1-\varphi)^2}}{2\kappa^{3/2}(1-\varphi)} \qquad (\kappa \gg 1) \tag{A.8}$$

(here the starting point is set to 0, but the result holds for all z_0 not too close to 1). This relation is valid for any $0 < \varphi < 1$. Setting formally $\varphi = 0$, one gets the relation which is twice larger than the asymptotic Eq. (39) derived for $\varphi = 0$. The missing factor 2 can be retrieved from the ratio in front of the first integral in Eq. (A.1). The difference between the cases $\varphi = 0$ and $\varphi > 0$ (small but strictly positive) can also be explained by the following argument. For non-symmetric case ($\varphi > 0$), the right endpoint $x_0 = L$ is closer to the minimum position $\hat{x}$ than the left endpoint $x_0 = -L$. When κ is large, the probability of large deviations from $\hat{x}$ rapidly decays with the distance so that the probability of exiting through the

left endpoint is exponentially smaller than that from the right endpoint. In other words, the above relation essentially describes the mean exit time from the right endpoint. In turn, when $\varphi = 0$ (and thus $\hat{x} = 0$), both endpoints are equivalent that doubles the chances to exit and thus twice reduces the mean exit time.

(iii) In the marginal case $\varphi = 1$, the integral in Eq. (A.5) grows logarithmically with κ. One can split the integral by an intermediate point $\bar{z} \gg 1$ so that

$$\int_0^{\bar{z}} dz\ e^{z^2}\ \mathrm{erfc}(z) + \int_{\bar{z}}^{\sqrt{\kappa}(1-z_0)} dz\ e^{z^2}\ \mathrm{erfc}(z) \simeq \frac{1}{\sqrt{\pi}} \ln \frac{\sqrt{\kappa}(1-z_0)}{c(\bar{z})},$$

where

$$c(\bar{z}) \equiv \bar{z} \exp\left(-\sqrt{\pi} \int_0^{\bar{z}} dz\ e^{z^2}\ \mathrm{erfc}(z) \right) \longrightarrow 0.375\ldots \quad (\bar{z} \to \infty).$$

We get therefore

$$\langle \tau \rangle_{z_0} \simeq \frac{L^2}{D}\ \frac{1}{2\kappa} \ln \frac{\sqrt{\kappa}(1-z_0)}{0.375\ldots} \qquad (\kappa \gg 1). \tag{A.9}$$

This asymptotic relation is accurate starting from $\sqrt{\kappa}(1-z_0) \gtrsim 2$.

Appendix A.2. Eigenvalues (interior problem)

For large κ, we search for positive solutions α_n of the equation $M(-\frac{\alpha_n^2}{4\kappa}, b, \kappa) = 0$ in the form: $\alpha_n^2/(4\kappa) = n - \varepsilon$, where ε is a small parameter, and $n = 0, 1, 2, \ldots$ One gets then

$$\begin{aligned} 0 = M\left(-n+\varepsilon; b; \kappa\right) &\simeq \sum_{j=0}^{n} \frac{(-n)(-n+1)\ldots(-n+j-1)\kappa^j}{b^{(j)}\ j!} \\ &\quad + \varepsilon(-1)^n n! \sum_{j=n+1}^{\infty} \frac{(-n+j-1)!\ \kappa^j}{b^{(j)}\ j!} + O(\varepsilon^2), \end{aligned}$$

from which the small parameter ε can be determined as

$$\varepsilon \simeq -\frac{S_1}{(-1)^n n! S_2}, \tag{A.10}$$

where S_1 and S_2 denote two above sums. The second sum can be written as

$$S_2 = \sum_{j=n+1}^{\infty} \frac{(-n+j-1)!\ \kappa^j}{b^{(j)}\ j!} = \Gamma(b) \sum_{j=0}^{\infty} \frac{\kappa^{j+n+1}}{\Gamma(b+j+1+n)(j+1)\ldots(j+1+n)}.$$

This expression can be obtained by integrating $n+1$ times the Mittag-Leffler function $E_{1,b+n+1}(\kappa)$ which asymptotically behaves as $E_{1,b+n+1}(\kappa) \simeq \kappa^{-b-n} e^{\kappa}(1 + O(1/\kappa))$ as $\kappa \gg 1$. Since the integration does not change the leading term, one concludes that

$$S_2 \simeq \Gamma(b) \kappa^{-b-n} e^{\kappa}(1 + O(1/\kappa)) \qquad (\kappa \gg 1).$$

Keeping the highest-order term in the first sum, $S_1 \simeq (-1)^n \kappa^n / b^{(n)}$, one gets

$$\varepsilon \simeq -\frac{\kappa^{b+2n}}{n!\Gamma(b+n)} e^{-\kappa},$$

from which we obtain the asymptotic behavior of the positive solution α_n as $\kappa \gg 1$:

$$\alpha_n^2 \simeq 4\kappa\Big[n + \frac{\kappa^{b+2n}e^{-\kappa}}{n!\Gamma(b+n)}\Big] \qquad (n = 0, 1, 2, \ldots). \tag{A.11}$$

In particular, the smallest solution α_0 exponentially decays with κ,

$$\alpha_0^2 \simeq \frac{4\kappa^{1+b}}{\Gamma(b)}\, e^{-\kappa} \qquad (\kappa \gg 1), \tag{A.12}$$

while the other eigenvalues grow linearly with κ:

$$\alpha_n^2 \simeq 4\kappa n \qquad (\kappa \gg 1,\ n = 1, 2, \ldots), \tag{A.13}$$

and the first-order correction ε decays exponentially fast. This asymptotic behavior can be related to equidistant energy levels of a quantum harmonic oscillator (see Appendix D).

Since α_0 rapidly vanishes, the first eigenfunction approaches the unity: $M(-\frac{\alpha_0^2}{4\kappa}, \frac{d}{2}, \kappa z^2) \to 1$. As a consequence, the normalization constant is simply $\beta_0^2 \approx 2\kappa^{d/2}/\Gamma(d/2)$ so that $w_0 \simeq 1$, because $M(1, b, z) = \Gamma(b)E_{1,b}(z)$.

Appendix A.3. Eigenvalues (exterior problem)

For the exterior problem, we consider the asymptotic behavior of solutions of $U(-\frac{\alpha^2}{4\kappa}, b, \kappa) = 0$ as $\kappa \to 0$. For non-integer b, one can use Eq. (87) to write in the lowest order in κ

$$0 = U\Big(-\frac{\alpha^2}{4\kappa}, b, \kappa\Big) \simeq \frac{\Gamma(1-b)}{\Gamma(1-b-\frac{\alpha^2}{4\kappa})} + \frac{\Gamma(b-1)}{\Gamma(-\frac{\alpha^2}{4\kappa})}\kappa^{1-b}. \tag{A.14}$$

For $b < 1$, κ^{1-b} is a small parameter so that the first term has to be small. Setting $1 - b - \frac{\alpha^2}{4\kappa} = -n + \varepsilon$ (with $n = 0, 1, 2, \ldots$) one gets

$$\varepsilon = (-1)^{n-1}\frac{\Gamma(b-1)}{n!\ \Gamma(b-1-n)\Gamma(1-b)}\ \kappa^{1-b}, \tag{A.15}$$

from which

$$\alpha_n^2 \simeq 4\kappa\Big(1 - b + n + \frac{(-1)^n\Gamma(b-1)}{n!\ \Gamma(b-1-n)\Gamma(1-b)}\ \kappa^{1-b} + \ldots\Big). \tag{A.16}$$

In turn, if $b > 1$, κ^{1-b} is a large parameter so that the second term has to be small. Setting $-\frac{\alpha^2}{4\kappa} = -n + \varepsilon$, one gets

$$\varepsilon = (-1)^{n-1}\frac{\Gamma(1-b)}{n!\ \Gamma(1-b-n)\Gamma(b-1)}\ \kappa^{b-1}, \tag{A.17}$$

from which

$$\alpha_n^2 \simeq 4\kappa\Big(n + \frac{(-1)^n\Gamma(1-b)}{n!\ \Gamma(1-b-n)\Gamma(b-1)}\ \kappa^{b-1} + \ldots\Big). \tag{A.18}$$

For integer b, the analysis is more subtle and is beyond the scope of this paper. We just checked numerically that $\alpha_0^2 \propto \kappa^b$ as $\kappa \to 0$ for $b = 1$ and $b = 2$ that corresponds to dimensions $d = 2$ and $d = 4$.

Appendix B. Confluent hypergeometric functions

For the sake of completeness, we summarize selected relations between special functions that are often used to describe first passage times of Ornstein-Uhlenbeck processes (see [68] for details). After that, we describe a rapidly converging representation of confluent hypergeometric functions.

Appendix B.1. Relations

The Kummer confluent hypergeometric function $M(a,b,z) = {}_1F_1(a;b;z)$ defined in Eq. (42), satisfies the Kummer's equation:

$$zy'' + (b-z)y' - ay = 0. \tag{B.1}$$

For $b = 1/2$, this equation is also related to the Weber's equation

$$y'' - (z^2/4 + c)y = 0, \tag{B.2}$$

which has two independent solutions: $e^{-z^2/4}M(c/2+1/4, 1/2, z^2/2)$ (even) and $ze^{-z^2/4}M(c/2+3/4, 3/2, z^2/2)$ (odd). These solutions are often expressed through the parabolic cylinder function $D_\nu(z)$, which satisfies Eq. (B.2) with $\nu = -c - 1/2$:

$$\begin{aligned} D_\nu(z) &= \frac{\cos(\frac{\pi\nu}{2})\Gamma(\frac{1+\nu}{2})}{\sqrt{\pi}\ 2^{-\nu/2}}\ e^{-z^2/4}\ M\left(-\frac{\nu}{2}, \frac{1}{2}, \frac{z^2}{2}\right) \\ &+ \frac{\sin(\frac{\pi\nu}{2})\Gamma(\frac{2+\nu}{2})}{\sqrt{\pi}\ 2^{-(\nu+1)/2}}\ e^{-z^2/4}\ zM\left(-\frac{\nu}{2}+\frac{1}{2}, \frac{3}{2}, \frac{z^2}{2}\right) \end{aligned} \tag{B.3}$$

$$= 2^{\nu/2}e^{-z^2/4}U\left(-\frac{\nu}{2}, \frac{1}{2}, \frac{z^2}{2}\right) \tag{B.4}$$

(the last relation is valid only for $\Re\{z\} \geq 0$).

The confluent hypergeometric functions $M(a,b,z)$ and $U(a,b,z)$ are also related to the Whittaker functions $M_{a,b}(z)$ and $W_{a,b}(z)$ [68]

$$\begin{aligned} M_{a,b}(z) &= e^{-z/2}z^{b+1/2}\ M(1/2+b-a, 1+2b, z), \\ W_{a,b}(z) &= e^{-z/2}z^{b+1/2}\ U(1/2+b-a, 1+2b, z). \end{aligned}$$

The following relations help to analyze the Brownian motion limit [39]

$$\lim_{\kappa\to 0} M\left(\frac{a}{4\kappa}, b+1, \kappa x\right) = 2^b\Gamma(b+1)\frac{I_b(\sqrt{xa})}{(xa)^{b/2}}, \tag{B.5}$$

$$\lim_{\kappa\to 0} \kappa^b\Gamma\left(\frac{a}{4\kappa}\right) U\left(\frac{a}{4\kappa}, b+1, \kappa x\right) = 2^{1-b}\frac{K_b(\sqrt{xa})}{(x/a)^{b/2}}, \tag{B.6}$$

where $I_\nu(z)$ and $K_\nu(z)$ are the modified Bessel functions of the first and second kind, respectively.

The asymptotic expansions for large $|z|$ (and fixed a and b) are [68] (Sec. 13.5):

$$M(a,b,z) \simeq \frac{e^z z^{a-b}\Gamma(b)}{\Gamma(a)}\left(\sum_{n=0}^{N_1-1}\frac{(b-a)^{(n)}(1-a)^{(n)}}{n!\ z^n} + O(|z|^{-N_1})\right) \tag{B.7}$$

$$+\ \frac{e^{\pm\pi i a}z^{-a}\Gamma(b)}{\Gamma(b-a)}\left(\sum_{n=0}^{N_2-1}\frac{(a)^{(n)}(1+a-b)^{(n)}}{n!\ (-z)^n}+O(|z|^{-N_2})\right),$$

$$U(a,b,z)\ \simeq z^{-a}\left(\sum_{n=0}^{N-1}\frac{(a)^{(n)}(1+a-b)^{(n)}}{n!\ (-z)^n}+O(|z|^{-N})\right)\quad(|\arg(z)|<3\pi/2),\tag{B.8}$$

where the upper [resp., lower] sign in the second line is taken if $-\pi/2<\arg(z)<3\pi/2$ [resp., $-3\pi/2<\arg(z)\le-\pi/2$], and N, N_1, and N_2 are truncation orders.

Appendix B.2. Computation

Series representations. The computation of the Kummer function $M(a,b,z)$ by direct series summation in Eq. (42) is not convenient for large $|a|$. For this case, two equivalent representations were proposed:

(i) $$M(a,b,z)=\Gamma(b)e^{z/2}2^{b-1}\sum_{n=0}^{\infty}A_n z^n\frac{J_{b-1+n}(\sqrt{z(2b-4a)})}{(\sqrt{z(2b-4a)})^{b-1+n}},\tag{B.9}$$

where the coefficients A_n are defined by

$$A_0=1,\quad A_1=0,\quad A_2=b/2,\quad nA_n=(n-2+b)A_{n-2}+(2a-b)A_{n-3}$$

(see [68], Sec. 13.3.7, and [138], Sec. 4.8). Note that the coefficients A_n depend on a and grow with $|a|$.

(ii) $$M(a,b,z)=\Gamma(b)e^{z/2}2^{b-1}\sum_{n=0}^{\infty}p_n(b,z)\frac{J_{b-1+n}(\sqrt{z(2b-4a)})}{(\sqrt{z(2b-4a)})^{b-1+n}},\tag{B.10}$$

where $p_n(b,z)$ are the Buchholz polynomials in b and z (see [139], Sec. 7.4). These polynomials are less explicit than the coefficients A_n, but they are independent of a. As a consequence, this representation is particularly convenient for large $|a|$.

The recurrence relations for the Buchholz polynomials were derived in [140]:

$$p_n(b,z)=\frac{(iz)^n}{n!}\sum_{k=0}^{[n/2]}\binom{n}{2k}f_k(b)g_{n-2k}(z),\tag{B.11}$$

where the polynomials $f_k(b)$ and $g_k(z)$ are defined recursively by

$$f_k(b)=\ -\left(\frac{b}{2}-1\right)\sum_{j=0}^{k-1}\binom{2k-1}{2j}\frac{4^{k-j}|B_{2(k-j)}|}{k-j}\ f_j(b),\quad f_0(b)=1,\tag{B.12}$$

$$g_k(z)=\ -\frac{iz}{4}\sum_{j=0}^{[(k-1)/2]}\binom{k-1}{2j}\frac{4^{j+1}|B_{2(j+1)}|}{j+1}\ g_{k-2j-1}(z),\quad g_0(z)=1,\tag{B.13}$$

and B_{2j} are the Bernoulli numbers. Using the recurrence relations between Bessel functions, $\frac{2\nu}{x}J_\nu(x)=J_{\nu-1}(x)+J_{\nu+1}(x)$, one can express

$$J_{b-1+n}(x)=P_n(1/x)J_{b-1}(x)+Q_n(1/x)J_b(x),$$

where the polynomials $P_n(z)$ and $Q_n(z)$ are defined recursively

$$P_0(z)=1,\quad P_1(z)=0,\quad P_{n+1}(z)=2(b-1+n)zP_n(z)-P_{n-1}(z),$$
$$Q_0(z)=0,\quad Q_1(z)=1,\quad Q_{n+1}(z)=2(b-1+n)zQ_n(z)-Q_{n-1}(z).$$

We get therefore the following expansion which rapidly converges for large x and moderate z:

$$M(a,b,z) = e^{z/2} \sum_{n=0}^{\infty} p_n(b,z) \left[F_b(x) \frac{P_n(1/x)}{x^n} + G_b(x) \frac{Q_n(1/x)}{x^{n-1}} \right], \qquad \text{(B.14)}$$

where $x = \sqrt{z(2b-4a)}$, and

$$F_b(x) = \Gamma(b) 2^{b-1} x^{1-b} J_{b-1}(x), \qquad G_b(x) = \Gamma(b) 2^{b-1} x^{-b} J_b(x). \qquad \text{(B.15)}$$

In particular, for $b = d/2$, one has

d	$F_b(x)$	$G_b(x)$
1	$\cos(x)$	$\sin(x)/x$
2	$J_0(x)$	$J_1(x)/x$
3	$\sin(x)/x$	$(\sin(x) - x\cos(x))/x^3$

(B.16)

The above recursive relations allow one to compute rapidly the polynomials $p_n(b,z)$, $P_n(1/x)$ and $Q_n(1/x)$. The series (B.14) can be truncated after 5-10 terms when $|az|$ is large enough, and z is not too large (see [140] for several examples).

According to Eq. (87), one can apply this method to compute the Tricomi confluent hypergeometric function $U(a,b,z)$ for non-integer b. Other series expansions for $U(a,b,z)$ are discussed in [141, 142]. For integer b, one can substitute $b_\varepsilon = b + \varepsilon$ into Eq. (87) and then take the limit $\varepsilon \to 0$. This extension by continuity yields [68]

$$U(a,b,z) = \frac{(-1)^b}{(b-1)!\,\Gamma(a-b+1)} \Bigg\{ M(a,b,z) \ln z + \frac{(b-2)!}{\Gamma(a)} \sum_{k=0}^{b-2} \frac{(a-b+1)^{(k)} z^{k-b+1}}{k!\,(2-b)^{(k)}} + \sum_{k=0}^{\infty} \frac{a^{(k)} z^k}{k!\,b^{(k)}} \Big(\psi(a+k) - \psi(1+k) - \psi(b+k) \Big) \Bigg\}, \qquad b = 1, 2, \ldots,$$

where $\psi(z) = \Gamma'(z)/\Gamma(z)$ is the digamma function, and the intermediate sum is omitted for $b = 1$. In practice, one can apply the above numerical scheme to rapidly compute $U(a, b_\varepsilon, z)$ through $M(a, b_\varepsilon, z)$ with several non-integer b_ε approaching the integer b, and then to extrapolate them in the limit $b_\varepsilon \to b$.

Taking the derivative of Eq. (B.10) with respect to a and using the relation $J'_\nu(x) = \frac{\nu}{x} J_\nu(x) - J_{\nu+1}(x)$, one obtains

$$\frac{\partial}{\partial a} M(a,b,z) = \Gamma(b) e^{z/2} 2^b z \sum_{n=0}^{\infty} p_n(b,z) \frac{J_{b+n}(\sqrt{z(2b-4a)})}{(\sqrt{z(2b-4a)})^{b+n}} \qquad \text{(B.17)}$$

or, equivalently,

$$\frac{\partial}{\partial a} M(a,b,z) = 2z e^{z/2} \sum_{n=0}^{\infty} p_n(b,z) \left[F_b(x) \frac{P_{n+1}(1/x)}{x^{n+1}} + G_b(x) \frac{Q_{n+1}(1/x)}{x^n} \right], \qquad \text{(B.18)}$$

with $x = \sqrt{z(2b-4a)}$. This expression allows one to rapidly compute the coefficients w_n in the spectral representation of the survival probability. Similar relation can be derived for $\frac{\partial}{\partial a} U(a,b,z)$ using Eq. (87) for non-integer b. Finally, one can also apply these formulas for computing the parabolic cylinder function $D_\nu(z)$ and its derivative $\frac{\partial}{\partial \nu} D_\nu(z)$ which are used to characterize the first passage time to a single barrier (Appendix C).

Integral representations. The above scheme is convenient for large $|a|$ and moderate $|z|$. However, if $|a|$ is moderate while $|z|$ is large, the numerical convergence of the above series is slowed down due to a rapid growth of Buchholz polynomials with z. In addition, the computation of the Tricomi function $U(a,b,z)$ as a linear combination (87) of two large Kummer functions can result in significant round-off errors at large z. In this case, one can apply a different technique which relies on integral representations of confluent hypergeometric functions.

For the Kummer function $M(a,b,z)$, one can use the following integral representation for $\Re\{b-a\}>0$ ‖

$$M(a,b,z)=\frac{e^z z^{\frac{1-b}{2}}\Gamma(b)}{\Gamma(b-a)}\int\limits_0^\infty dt\; e^{-t}\; t^{\frac{b-1}{2}-a}\; J_{b-1}(2\sqrt{zt}). \tag{B.19}$$

This representation is convenient for computing eigenvalues and eigenfunctions because $a=-\alpha^2/(4\kappa)<0$ and $b=d/2>0$.

The Tricomi function $U(a,b,z)$ has an integral representation for positive a [68]

$$U(a,b,z)=\frac{1}{\Gamma(a)}\int\limits_0^\infty dt\, e^{-zt}\, t^{a-1}\,(1+t)^{b-a-1}\quad(\Re\{a\}>0,\Re\{z\}>0). \tag{B.20}$$

When a is negative, one can use the recurrence relation to increase a:

$$U(a-1,b,z)+(b-2a-z)U(a,b,z)+a(a+1-b)U(a+1,b,z)=0. \tag{B.21}$$

Applying this relation repeatedly, one gets

$$U(a,b,z)=p_n(a,b,z)U(a+n,b,z)+q_n(a,b,z)U(a+n+1,b,z), \tag{B.22}$$

where the polynomials $p_n(a,b,z)$ and $q_n(a,b,z)$ can be rapidly computed through recurrence relations:

$$\begin{aligned} p_n(a,b,z) &= q_{n-1}(a,b,z)-(b-2(a+n)-z)p_{n-1}(a,b,z), \qquad p_0=1,\\ q_n(a,b,z) &= -(a+n)(a+n+1-b)p_{n-1}(a,b,z), \qquad q_0=0. \end{aligned}$$

Choosing n such that $a+n>0$, one can express $U(a,b,z)$ in terms of $U(a+n,b,z)$ and $U(a+n+1,b,z)$ which are found by numerical integration of Eq. (B.20). If z is too large, it is convenient to divide each recurrence relation by z and to consider them as polynomials of $1/z$. The resulting value can be compared with the asymptotic expansion (B.8).

Appendix C. First passage time to a single barrier

The first passage times (one-barrier problem) for harmonically trapped particles have attracted more attention than the first exit times (two-barrier problem) [29, 32, 33, 34, 35, 36]. In general, the first passage time τ_ℓ to a single barrier at $\ell>0$ in one dimension can be found following the steps from Sec. 2.6. In practice, these results can be deduced

‖ See `http://dlmf.nist.gov/13.16.E3`

from the FET statistics. If the starting point x_0 lies on the right to ℓ (i.e., $x_0 > \ell$), this problem is equivalent to the exterior problem to reach the interval $[-\ell, \ell]$ from outside (see Sec. 2.9). In turn, if $0 < x_0 < \ell$, the FPT to a single barrier ℓ can be deduced from the FET from the interval $[-a, \ell]$ in the limit $a \to \infty$.

In order to illustrate this point, we focus on the moment-generating function $\tilde{q}(x_0, s)$ given by Eq. (60), with $\ell = L(1-\varphi)$ and $a = L(1+\varphi)$. Setting $1-\varphi = \varepsilon$, we consider the limit $\varepsilon \to 0$, for which $L = \ell/\varepsilon \to \infty$ and $1-\varphi = \varepsilon \to 0$ so that $a \to \infty$ while ℓ is kept fixed. The asymptotic behavior of functions $m^{(1,2)}_{\alpha,\kappa}$ from Eq. (43) as $\varepsilon \to 0$ can be easily found:

$$
\begin{aligned}
m^{(1)}_{\alpha,\kappa}(1-\varphi) &\simeq M\Big(a, \frac{1}{2}, y\Big), \\
m^{(2)}_{\alpha,\kappa}(1-\varphi) &\simeq \varepsilon M\Big(a+\frac{1}{2}, \frac{3}{2}, y\Big), \\
m^{(1)}_{\alpha,\kappa}(-1-\varphi) &\simeq \frac{\Gamma(1/2)}{\Gamma(a)}(4y/\varepsilon^2)^{a-1/2} e^{4y/\varepsilon^2}, \\
m^{(2)}_{\alpha,\kappa}(-1-\varphi) &\simeq -2\frac{\Gamma(3/2)}{\Gamma(a+1/2)}(4y/\varepsilon^2)^{a-1} e^{4y/\varepsilon^2},
\end{aligned}
$$

where we replaced α and κ by $-Ds/L^2$ and $kL^2/(2D\gamma)$, introduced short notations $a = s\gamma/(2k)$ and $y = k\ell^2/(2D\gamma)$, and used the asymptotic relation (B.7) for the last two functions. Substituting the above expressions into Eq. (60), one deduces in the limit $\varepsilon \to 0$

$$
\tilde{q}(x_0, s) = \frac{M(a, \frac{1}{2}, y_0) + 2\frac{\Gamma(a+1/2)}{\Gamma(a)}\sqrt{y_0} M(a+1/2, \frac{3}{2}, y_0)}{M(a, \frac{1}{2}, y) + 2\frac{\Gamma(a+1/2)}{\Gamma(a)}\sqrt{y} M(a+1/2, \frac{3}{2}, y)}, \tag{C.1}
$$

where $y_0 = kx_0^2/(2D\gamma)$. Using Eq. (B.3), one can alternatively write the moment-generating function as

$$
\tilde{q}(x_0, s) = \exp\left(\frac{k(x_0^2 - \ell^2)}{4D\gamma}\right) \frac{D_{-s\gamma/k}\Big(-x_0\sqrt{\frac{k}{D\gamma}}\Big)}{D_{-s\gamma/k}\Big(-\ell\sqrt{\frac{k}{D\gamma}}\Big)} \qquad (0 \le x_0 \le \ell). \tag{C.2}
$$

Note also that Eq. (88) for the exterior case $x_0 > \ell$ can also be written in terms of the parabolic cylinder function $D_\nu(z)$ according to Eq. (B.4):

$$
\tilde{q}(x_0, s) = \exp\left(\frac{k(x_0^2 - \ell^2)}{4D\gamma}\right) \frac{D_{-s\gamma/k}\Big(x_0\sqrt{\frac{k}{D\gamma}}\Big)}{D_{-s\gamma/k}\Big(\ell\sqrt{\frac{k}{D\gamma}}\Big)} \qquad (x_0 > \ell), \tag{C.3}
$$

in agreement with [39] (see also [42, 32]).

The inverse Laplace transform yields the probability density $p_{x,a}(t)$ [42, 35]

$$
q(x_0, t) = -\frac{k}{\gamma}\exp\left(\frac{k(x_0^2 - \ell^2)}{4D\gamma}\right) \sum_{n=1}^{\infty} \frac{D_{\nu_n}\Big(\pm x_0\sqrt{\frac{k}{D\gamma}}\Big)}{D'_{\nu_n}\Big(\pm\ell\sqrt{\frac{k}{D\gamma}}\Big)} e^{-\nu_n k t/\gamma}, \tag{C.4}
$$

where $0 < \nu_1 < ... < \nu_n < ...$ are the zeros of the function $D_\nu(\pm\ell\sqrt{k/(D\gamma)})$, and $D'_{\nu_n}(z)$ is the derivative of $D_\nu(z)$ with respect to ν, evaluated at point $\nu = \nu_n$ [42] (p. 154). The

signs plus and minus correspond to $x_0 > \ell$ and $x_0 < \ell$, respectively. Both $D_\nu(z)$ and $D'_\nu(z)$ can be rapidly evaluated by the numerical scheme presented in Appendix B.2.

In the special case $\ell = 0$, the FET probability density gets a simple explicit form:

$$q(x_0,t) = \frac{x_0}{\sqrt{4\pi D}}\left(\frac{k/\gamma}{\sinh(kt/\gamma)}\right)^{3/2}\exp\left(-\frac{kx_0^2}{4D\gamma}\frac{e^{-kt/\gamma}}{\sinh(kt/\gamma)}+\frac{kt}{2\gamma}\right). \quad \text{(C.5)}$$

In the limit $k \to 0$, one retrieves the classical formula for the FPT of Brownian motion at the origin

$$q(x_0,t) = \frac{x_0}{\sqrt{4\pi D t^3}}\exp\left(-\frac{x_0^2}{4Dt}\right) \qquad (k=0). \quad \text{(C.6)}$$

Appendix D. Quantum harmonic oscillator

The eigenvalue problem (40) with $b = 1/2$ is closely related to eigenstates of a quantum harmonic oscillator of mass m and frequency ω [120]. In fact, the eigenstates ψ_n and energies E_n of the Hamiltonian $H = \frac{\hat{p}^2}{2m}+\frac{m\omega^2 x^2}{2m}$ satisfy the time-independent Schrödinger equation

$$\Big[-\frac{\hbar^2}{2m}\partial_x^2+\frac{m\omega^2x^2}{2}\Big]\psi(x) = E\psi(x), \quad \text{(D.1)}$$

where $\hat{p} = -i\hbar\partial_x$ is the momentum operator, and $\hbar$ is the (reduced) Planck constant. In terms of the dimensionless coordinate $z = x\sqrt{2m\omega/\hbar}$, the above Schrödinger equation is reduced to the Weber's equation (B.2), with $c = -\frac{E}{\hbar\omega}$. Setting $\psi(z) = e^{-z^2/4}\tilde{u}(z)$ yields $\tilde{u}'' - z\tilde{u}' - (c+1/2)\tilde{u} = 0$, from which the rescaling $u(x) = \tilde{u}(\sqrt{k/(D\gamma)}(x-\hat{x}))$ implies Eq. (40), with $\lambda = -\frac{k}{\gamma}(c+1/2)$. As a consequence, the energies of the quantum oscillator and the eigenvalues of the FP operator are simply related as: $\lambda = \frac{k}{\gamma}(\frac{E}{\hbar\omega}-\frac{1}{2})$.

If no boundary condition is imposed, the non-normalized eigenstate is simply $\psi(x) = D_\nu(x\sqrt{2m\omega/\hbar})$, where $D_\nu(z)$ is the parabolic cylinder function (see Appendix B.1), and $\nu = -c-1/2$. One can check that

$$D_\nu(z) \simeq e^{-z^2/4}z^\nu\Big[1-\frac{\nu(\nu-1)}{2z^2}+O(z^{-4})\Big] \qquad (z \gg 1), \quad \text{(D.2)}$$

$$D_\nu(z) \simeq e^{-z^2/4}z^\nu\Big[1-\frac{\nu(\nu-1)}{2z^2}+O(z^{-4})\Big] \quad \text{(D.3)}$$

$$-\frac{\sqrt{2\pi}}{\Gamma(-\nu)}e^{\pi i\nu}e^{z^2/4}z^{-\nu-1}\Big[1+\frac{(\nu+1)(\nu+2)}{2z^2}+O(z^{-4})\Big] \quad (z \ll -1).$$

In order to eliminate the unphysical rapid growth of the eigenstate as $z \to -\infty$, one needs to impose $\nu = n$ with $n = 0, 1, 2, \ldots$ to remove the last term, from which one retrieves the quantized energies of the quantum harmonic oscillator: $E_n = \hbar\omega(n+1/2)$, while the eigenfunctions become expressed through the Hermite polynomials $H_n(z)$

$$\psi_n(x) = \frac{1}{\sqrt{2^n n!}}\left(\frac{m\omega}{\pi\hbar}\right)^{1/4}\exp\left(-\frac{m\omega x^2}{2\hbar}\right)H_n\left(\sqrt{\frac{m\omega}{\hbar}}x\right),$$

where the usual normalization prefactor is included, and we used $D_n(z) = 2^{-n/2}e^{-z^2/4}H_n(z/\sqrt{2})$. Since imposing no boundary condition corresponds to barriers

at distance $L \to \infty$, we retrieve the asymptotic behavior $\lambda_n \simeq \frac{k}{\gamma} n$ or, equivalently, $\alpha_n^2 = \frac{L^2}{D}\lambda_n \simeq 2\kappa n$ as $\kappa \to \infty$. Note that the prefactor 2κ is twice smaller than that of Eq. (A.13) because the latter relation accounts only for symmetric eigenfunctions that contribute to the survival probability.

Imposing Dirichlet boundary condition at $x = \pm L$ corresponds to setting infinite potential outside the interval $[-L, L]$ (and keeping the harmonic potential inside). The eigenvalue problem for a quantum oscillator in such potential is equivalent to the analysis of the first exit time distribution in Sec. 2.6.

[1] Redner S 2001 *A Guide to First Passage Processes* (Cambridge: Cambridge University press)

[2] Metzler R, Oshanin G, and Redner S (Eds.) 2014 *First-Passage Phenomena and Their Applications* (Singapore: World Scientific).

[3] Bénichou O and Voituriez R 2014, From first-passage times of random walks in confinement to geometry-controlled kinetics, *Phys. Rep.* **539** 225-284

[4] Bouchaud J-P and Georges A 1990, Anomalous diffusion in disordered media: Statistical mechanisms, models and physical applications, *Phys. Rep.* **195** 127-293

[5] Metzler R and Klafter J 2000, The random walk's guide to anomalous diffusion: a fractional dynamics approach, *Phys. Rep.* **339** 1-77

[6] Metzler R and Klafter J 2004, The restaurant at the end of the random walk: recent developments in the description of anomalous transport by fractional dynamics, *J. Phys. A: Math. Gen.* **37** R161-R208

[7] Condamin S, Bénichou O, and Klafter J 2007, First-Passage Time Distributions for Subdiffusion in Confined Geometry, *Phys. Rev. Lett.* **98** 250602

[8] Yuste SB and Lindenberg K 2007, Subdiffusive target problem: Survival probability, *Phys. Rev. E* **76** 051114

[9] Yuste SB, Oshanin G, Lindenberg K, Bénichou O, and Klafter J 2008, Survival probability of a particle in a sea of mobile traps: A tale of tails, *Phys. Rev. E* **78** 021105

[10] Grebenkov DS 2010, Searching for partially reactive sites: Analytical results for spherical targets, *J. Chem. Phys.* **132** 034104

[11] Grebenkov DS 2010, Subdiffusion in a bounded domain with a partially absorbing-reflecting boundary, *Phys. Rev. E* **81** 021128

[12] Molchan GM 1999, Maximum of a Fractional Brownian Motion: Probabilities of Small Values, *Commun. Math. Phys.* **205** 97-111

[13] Likthman AE and Marques CM 2006, First-passage problem for the Rouse polymer chain: An exact solution, *Europhys. Lett.* **75** 971-977

[14] Jeon J-H, Chechkin AV, and Metzler R 2011, First passage behaviour of fractional Brownian motion in two-dimensional wedge domains, *EuroPhys. Lett.* **94**, 20008

[15] Sanders LP and Ambjörnsson T 2012, First passage times for a tracer particle in single file diffusion and fractional Brownian motion, *J. Chem. Phys.* **136** 175103

[16] Koren T, Lomholt MA, Chechkin AV, Klafter J, and Metzler R 2007, Leapover Lengths and First Passage Time Statistics for Levy Flights, *Phys. Rev. Lett.* **99** 160602

[17] Koren T, Klafter J, and Magdziarz M 2007, First passage times of Levy flights coexisting with subdiffusion, *Phys. Rev. E* **76** 031129

[18] Tejedor V, Bénichou O, Metzler R, and Voituriez R 2011, Residual mean first-passage time for jump processes: theory and applications to Lvy flights and fractional Brownian motion, *J. Phys. A* **44** 255003

[19] Bénichou O, Grebenkov DS, Levitz P, Loverdo C, and Voituriez R 2010, Optimal Reaction Time for Surface-Mediated Diffusion, *Phys. Rev. Lett.* **105** 150606

[20] Bénichou O, Grebenkov DS, Levitz P, Loverdo C, and Voituriez R 2011, Mean first-passage time

of surface-mediated diffusion in spherical domains, *J. Stat. Phys.* **142** 657-685
[21] Rupprecht J-F, Bénichou O, Grebenkov DS, and Voituriez R 2012, Kinetics of active surface-mediated diffusion in spherically symmetric domains, *J. Stat. Phys.* **147** 891-918
[22] Rupprecht J-F, Bénichou O, Grebenkov DS, and Voituriez R 2012, Exact mean exit time for surface-mediated diffusion, *Phys. Rev. E* **86** 041135
[23] Oshanin G, Lindenberg K, Wio HS, and Burlatsky S 2009, Efficient search by optimized intermittent random walks, *J. Phys. A* **42** 434008
[24] Bénichou O, Loverdo C, Moreau M, and Voituriez R 2011, Intermittent search strategies, *Rev. Mod. Phys.* **83** 81-130
[25] Condamin S, Bénichou O, Tejedor V, Voituriez R, and Klafter J 2007, First-passage time in complex scale-invariant media, *Nature* **450**, 77-80
[26] Condamin S, Tejedor V, Voituriez R, Bénichou O, and Klafter J 2008, Probing microscopic origins of confined subdiffusion by first-passage observables, *Proc. Nat. Acad. Sci. USA* **105** 5675-5680
[27] Holcman D, Marchewka A and Schuss Z 2005, Survival probability of diffusion with trapping in cellular neurobiology, *Phys. Rev. E* **72** 031910
[28] Crandall SH 1970, First crossing probabilities of the linear oscillator, *J. Sound. Vibr.* **12** 285-299
[29] Siegert AJF 1951, On the First Passage Time Probability Problem, *Phys. Rev.* **81** 617-623
[30] Darling DA and Siegert AJF 1953, The first passage problem for a continuous Markov process, *Ann. Math. Statist.* **24** 624-639
[31] Lindenberg K, Shuler KE, Freeman J, and Lie TJ 1975, First passage time and extremum properties of Markov and independent processes, *J. Stat. Phys.* **12** 217-251
[32] Ricciardi LM and Sato S 1988, First-Passage-Time Density and Moments of the Ornstein-Uhlenbeck Process, *J. Appl. Prob.* **25** 43-57
[33] Leblanc B, Renault O, and Scaillet O 2000, A correction note on the first passage time of an Ornstein-Uhlenbeck process to a boundary, *Finance Stochast.* **4** 109-111
[34] Göing-Jaeschke A and Yor M 2003, A clarification note about hitting times densities for Ornstein-Uhlenbeck processes, *Finance Stochast.* **7** 413-415
[35] Alili L, Patie P, and Pedersen JL 2005, Representations of the First Hitting Time Density of an Ornstein-Ohlenbeck Process, *Stoch. Models* **21** 967-980
[36] Yi C 2010, On the first passage time distribution of an Ornstein-Uhlenbeck process, *Quant. Finance* **10** 957-960
[37] Spendier K, Sugaya S, and Kenkre VM 2013, Reaction-diffusion theory in the presence of an attractive harmonic potential, *Phys. Rev. E* **88** 062142
[38] Toenjes R, Sokolov IM, and Postnikov EB 2013, Nonspectral Relaxation in One Dimensional Ornstein-Uhlenbeck Processes, *Phys. Rev. Lett.* **110** 150602
[39] Borodin AN and Salminen P 1996 *Handbook of Brownian Motion: Facts and Formulae* (Birkhauser Verlag, Basel-Boston-Berlin)
[40] Revuz D and Yor M 1999 *Continuous martingales and Brownian motion*, Third Ed. (Springer)
[41] Itô K and McKean HP 1996 *Diffusion Processes and Their Sample Paths* 2nd Ed. (Springer-Verlag, Berlin, Heidelberg).
[42] Jeanblanc M, Yor M, and Chesney M 2009 *Mathematical Methods For Financial Markets* (Springer-Verlag)
[43] Crank J 1975 *The Mathematics of Diffusion*, 2nd Ed. (Clarendon, Oxford)
[44] Carslaw HS and Jaeger JC 1959 *Conduction of Heat in Solids*, 2nd Ed. (Clarendon, Oxford)
[45] Hughes BD 1995 *Random Walks and Random Environments* (Clarendon Press, Oxford)
[46] Gardiner C 2004 *Handbook of Stochastic Methods for Physics, Chemistry and Natural Sciences* 3rd Ed. (Springer)
[47] Doob JL 1984 *Classical Potential Theory and Its Probabilistic Counterpart* (Springer, Verlag, Berlin, Heidelberg, and New York)
[48] van Kampen NG 2007 *Stochastic Processes in Physics and Chemistry*, 3ed. (Amsterdam: Elsevier)
[49] Uhlenbeck GE and Ornstein LS 1930, On the theory of the Brownian motion, *Phys. Rev.* **36** 823

[50] Wang MC and Uhlenbeck GE 1945, On the Theory of the Brownian Motion II, *Rev. Mod. Phys.* **17** 323
[51] Ricciardi LM and Sato S 1990, Diffusion processes anf first-passage-time problems, in *Lectures in Applied Mathematics and Informatics* ed. L. M. Ricciardi (Manchester University Press)
[52] Coffey WT, Kalmykov YP, and Waldron JT 2004 *The Langevin Equation: With Applications to Stochastic Problems in Physics, Chemistry and Electrical Engineering* 2nd Ed., World Scientific Publishing (Series in Contemporary Chemical Physics - Vol 14) (Singapore)
[53] Risken H 1996 *The Fokker-Planck equation: methods of solution and applications*, 3rd Ed. (Berlin: Springer)
[54] Kolpas A, Moehlis J and Kevrekidis IG 2007, Coarse-grained analysis of stochasticity-induced switching between collective motion states, *Proc. Nat. Acad. Sci.* **104** 5931-5935
[55] Grebenkov DS and Nguyen B-T 2013, Geometrical structure of Laplacian eigenfunctions, *SIAM Rev.* **55** 601-667
[56] Kac M 1949 On the distribution of certain Wiener functionals, *Trans. Am. Math. Soc.* **65** 1-13
[57] Kac M 1951, On some connections between probability theory and differential and integral equations, in *Proc. 2nd Berkeley Symp. Math. Stat. Prob.* edited by J. Neyman (University of California Press, Berkeley) 189-215
[58] Freidlin M 1985 *Functional Integration and Partial Differential Equations*, Annals of Mathematics Studies (Princeton University Press, Princeton, New Jersey)
[59] Simon B 1979 *Functional integration and quantum physics* (Academic press, London, New York, San Francisco)
[60] Bass RF 1998 *Diffusions and Elliptic Operators* (Springer, New York)
[61] Pontryagin L, Andronov A, and Witt A 1933, On the statistical treatment of dynamical systems, *Zh. Eksp. Teor. Fiz.* **3** 172 [Reprinted in *Noise in Nonlinear Dynamical Systems*, 1989, ed. by F. Moss and P. V. E. McClintock (Cambridge University Press, Cambridge), Vol. 1, p. 329]
[62] Castro LB and de Castro AS 2013, Trapping of a particle in a short-range harmonic potential well, *J. Math. Chem.* **51** 265-277
[63] Weiss GH 1981, First passage time problems for one-dimensional random walks, *J. Stat. Phys.* **24** 587-594
[64] Szabo A, Schulten K, and Schulten Z 1980, First passage time approach to diffusion controlled reactions, *J. Chem. Phys.* **72** 4350-4357
[65] Weiss GH 1986, Overview of theoretical models for reaction rates, *J. Stat. Phys.* **42** 3-36
[66] Hänggi P, Talkner P, and Borkovec M 1990, Reaction-rate theory: fifty years after Kramers, *Rev. Mod. Phys.* **62** 251-341
[67] Kramers HA 1940, Brownian motion in a field of force and the diffusion model of chemical reactions, *Physica* **7** 284
[68] Abramowitz M and Stegun IA 1965 *Handbook of Mathematical Functions* (Dover Publisher, New York)
[69] Rohrbach A, Tischer C, Neumayer D, Florin E-L, and Stelzer EHK 2004, Trapping and tracking a local probe with a photonic force microscope, *Rev. Sci. Instrum.* **75** 2197
[70] Lukić B, Jeney S, Sviben Z, Kulik AJ, Florin E-L, and Forró L 2007, Motion of a colloidal particle in an optical trap, *Phys. Rev. E* **76** 011112
[71] Franosch T, Grimm M, Belushkin M, Mor FM, Foffi G, Forró L, and Jeney S 2011, Resonances arising from hydrodynamic memory in Brownian motion, Nature **478** 85
[72] Huang R, Chavez I, Taute KM, Lukić B, Jeney S, Raizen MG, and Florin E-L 2011, Direct observation of the full transition from ballistic to diffusive Brownian motion in a liquid, *Nat. Phys.* **7** 576
[73] Bertseva E, Grebenkov DS, Schmidhauser P, Gribkova S, Jeney S, and Forró L 2012, Optical Trapping Microrheology in Cultured Human Cells, *Eur. Phys. J. E* **35** 63
[74] Grebenkov DS, Vahabi M, Bertseva E, Forró L, and Jeney S 2013, Hydrodynamic and subdiffusive motion of tracers in a viscoelastic medium, *Phys. Rev. E* **88** 040701(R)

[75] Ashkin A, Schütze K, Dziedzic JM, Euteneuer U, and Schliwa M 1990, Force generation of organelle transport measured in vivo by an infrared laser trap, *Nature* **348** 346-348
[76] Kuo SC and Sheetz MP 1993, Force of single kinesin molecules measured with optical tweezers, *Science* **260** 232-234
[77] Brangwynne CP, Koenderink GH, MacKintosh FC, and Weitz DA 2009, Intracellular transport by active diffusion, *Trends Cell. Biol.* **19** 423-427
[78] Sokolov IM 2012, Models of anomalous diffusion in crowded environments, *Soft Matter* **8** 9043-9052
[79] Bressloff PC and Newby JM 2013, Stochastic models of intracellular transport, *Rev. Mod. Phys.* **85** 135-196
[80] Desposito MA and Vinales AD 2009, Subdiffusive behavior in a trapping potential: Mean square displacement and velocity autocorrelation function, *Phys. Rev. E* **80** 021111
[81] Grebenkov DS 2011, Time-averaged quadratic functionals of a Gaussian process, *Phys. Rev. E* **83** 061117
[82] Bal G and Chou T 2004, On the reconstruction of diffusions from first-exit time distributions, *Inv. Problems* **20**, 1053-1065 (2004)
[83] Masson J-B, Casanova D, Türkcan S, Voisinne G, Popoff MR, Vergassola M, and Alexandrou A 2009, Inferring maps of forces inside cell membrane microdomains, *Phys. Rev. Lett.* **102**, 048103
[84] Kenwright DA, Harrison AW, Waigh TA, Woodman PG, and Allan VJ 2012, First-passage-probability analysis of active transport in live cells, *Phys. Rev. E* **86** 031910
[85] Lindner M, Nir G, Vivante A, Young IT, and Garini Y 2013, Dynamic analysis of a diffusing particle in a trapping potential, *Phys. Rev. E* **87** 022716
[86] Golding I and Cox EC 2006, Physical Nature of Bacterial Cytoplasm, *Phys. Rev. Lett.* **96** 098102
[87] Szymanski J and Weiss M 2009, Elucidating the Origin of Anomalous Diffusion in Crowded Fluids, *Phys. Rev. Lett.* **103** 038102
[88] Metzler R, Tejedor V, Jeon J-H, He Y, Deng WH, Burov S, and Barkai E 2009, Analysis of Single Particle Trajectories: From Normal to Anomalous Diffusion, *Acta Phys. Pol. B* **40** 1315
[89] Jeon J-H, Tejedor V, Burov S, Barkai E, Selhuber-Unkel C, Berg-Sørensen K, Oddershede L, and Metzler R 2011, In Vivo Anomalous Diffusion and Weak Ergodicity Breaking of Lipid Granules, *Phys. Rev. Lett.* **106** 048103
[90] Bell GI 1978, Models for the specific adhesion of cells to cells, *Science* **200** 618-627
[91] Evans E and Ritchie K 1997, Dynamic strength of molecular adhesion bonds, *Biophys. J.* **72** 1541-1555
[92] Izrailev S, Stepaniants S, Balsera M, Oono Y, and Schulten K 1997, Molecular dynamics study of unbinding of the avidin-biotin complex, *Biophys. J.* **72** 1568-1581
[93] Merkel R, Nassoy P, Leung A, Ritchie K, and Evans E 1999, Energy landscapes of receptor-ligand bonds explored with dynamic force spectroscopy, *Nature* **397** 50-53.
[94] Heymann B and Grubmüller H 2000, Dynamic Force Spectroscopy of Molecular Adhesion Bonds, *Phys. Rev. Lett.* **84** 6126-6129
[95] Evans E 2001, Probing the relation between force-lifetime-and chemistry in single molecular bonds, *Ann. Rev. Biophys. Biomol. Struct.* **30** 105-128
[96] Butt H-J, Cappella B, and Kappl M 2005, Force measurements with the atomic force microscope: Technique, interpretation and applications, *Surf. Sci. Rep.* **59** 1-152
[97] Box G, Jenkins GM, and Reinsel GC 1994 *Time Series Analysis: Forecasting and Control* Third ed. (Prentice-Hall)
[98] Covel MW 2009 *Trend Following (Updated Edition): Learn to Make Millions in Up or Down Markets* (Pearson Education, New Jersey)
[99] Clenow AF 2013 *Following the Trend: Diversified Managed Futures Trading* (Wiley & Sons, Chichester UK)
[100] Bouchaud J-P and Potters M 2003 *Theory of Financial Risk and Derivative Pricing: From*

Statistical Physics to Risk Management (Cambridge University Press)
[101] Chan LKC, Jegadeesh N, and Lakonishok J 1996, Momentum Strategies, *J. Finance* **51** 1681-1713
[102] Moskowitz TJ, Ooi YH, and Pedersen LH 2012, Time series momentum, *J. Finan. Econ.* **104** 228-250
[103] Asness CS, Moskowitz TJ, and Pedersen LH 2013, Value and momentum everywhere, *J. Finance* **68** 929-985
[104] Grebenkov DS and Serror J 2014, Following a Trend with an Exponential Moving Average: Analytical Results for a Gaussian Model, Physica A **394** 288-303
[105] Hull JC 2003 *Options, Futures and Other Derivatives* (Upper Saddle River, NJ: Prentice Hall).
[106] Vasicek O 1977, An Equilibrium Characterisation of the Term Structure, *J. Financ. Econom.* **5** 177-188
[107] Davydov D and Linetsky V 2003, Pricing Options on Scalar Diffusions: An Eigenfunction Expansion Approach, *Operations Research* **51** 185-209
[108] Tuckwell HC and Wan FYM 1984, First-passage time of Markov processes to moving barriers, *J. Appl. Prob.* **21** 695709
[109] Durbin J 1985, The first-passage density of a continuous Gaussian process to a general boundary, *J. Appl. Prob.* **22** 99-122
[110] Lerche HR 1986 *Boundary crossing of Brownian motion* (Vol. 40 of Lecture Notes in Statistics, Springer-Verlag, Berlin)
[111] Wang L and Pötzelberger K 1997, Boundary crossing probability for Brownian motion and general boundaries, *J. Appl. Prob.* **34** 54-65
[112] Kahale N 2008, Analytic Crossing Probabilities for Certain Barriers by Brownian Motion, *Ann. Appl. Probab.* **18** 1424-1440
[113] Breiman L 1966, First exit time from a square root boundary, *Proc 5th Berkeley Symp Math Statist Prob* **2** 9-16
[114] Shepp LA 1967, A first passage problem for the Wiener process, *Ann. Math. Statist.* **38** 1912-1914
[115] Novikov AA 1971, On stopping times for a Wiener process, *Theory Prob. Appl.* **16** 449-456
[116] Sato S 1977, Evaluation of the first passage probability to a square root boundary for the Wiener process, *J. Appl. Prob.* **14** 53-70
[117] Salminen P 1988, On the First Hitting Time and the Last Exit Time for a Brownian Motion to/from a Moving Boundary, *Adv. Appl. Prob.* **20** 411-426
[118] Novikov A, Frishling V and Kordzakhia N 1999, Approximations of boundary crossing probabilities for a Brownian motion, *J. Appl. Prob.* **36** 1019-1030
[119] De Long DM 1981, Crossing probability for a square root boundary by a bessel process, *Commun. Stat. Theory Meth.* **10** 2197-2213
[120] Merzbacher E 1998 *Quantum Mechanics* 3rd Ed (Wiley & Sons, New York)
[121] Griffiths DJ 2004 *Introduction to Quantum Mechanics* 2nd Ed (Prentice Hall, New Jersey)
[122] Caroli B, Caroli C, and Roulet B 1979, Diffusion in a Bistable Potential: A Systematic WKB Treatment, *J. Stat. Phys.* **21** 415-437
[123] van Kampen NG 1977, A Soluble Model for Diffusion in a Bistable Potential, *J. Stat. Phys.* **17** 71-88
[124] Mörsch M, Risken H, and Vollmer HD 1979, One-Dimensional Diffusion in Soluble Model Potentials, *Z. Phys. B* **32** 245-252
[125] Hongler MO and Zheng WM 1982, Exact Solution for the Diffusion in Bistable Potentials, *J. Stat. Phys.* **29** 317-327
[126] Voigtlaender K and Risken H 1985, Solutions of the Fokker-Planck equation for a double-well potential in terms of matrix continued fractions, *J. Stat. Phys.* **40** 397-429
[127] Jung P and Risken H 1985, Motion in a Double-Well Potential with Additive Colored Gaussian Noise, *Z. Phys. B: Conden. Mat.* **61** 367-379
[128] Ivlev BI 1988, On the dynamics of a particle in a two-well potential, *Sov. Phys. JETP* **68** 1486
[129] Kalmykov YP, Coffey WT and Titov SV 2006, Fractional translational diffusion of a Brownian

particle in a double well potential, *Phys. Rev. E* **74** 011105

[130] Gradshteyn IS and Ryzhik IM 1980 *Table of Integrals, Series, and Products*, (New York: Academic Press)

[131] Collins FC and Kimball GE 1949, Diffusion-controlled reaction rates, *J. Colloid Sci.* **4** 425-437

[132] Wilemski G and Fixman M 1973, General theory of diffusion-controlled reactions, *J. Chem. Phys.* **58**, 4009

[133] Sano H and Tachiya M 1979, Partially diffusion-controlled recombination, *J. Chem. Phys.* **71** 1276-1282

[134] Tachiya M 1983, Theory of diffusion-controlled reactions: Formulation of the bulk reaction rate in terms of the pair probability, *Radiat. Phys. Chem.* **21** 167-175

[135] Sapoval B 1994, General Formulation of Laplacian Transfer Across Irregular Surfaces, *Phys. Rev. Lett.* **73** 3314-3316

[136] Grebenkov DS 2006, Partially Reflected Brownian Motion: A Stochastic Approach to Transport Phenomena, in *Focus on Probability Theory* Ed. L. R. Velle, pp. 135-169 (Hauppauge NY: Nova Science Publishers)

[137] Singer A, Schuss Z, Osipov A, and Holcman D 2008, Partially reflected diffusion, *SIAM J. Appl. Math.* **68** 844-868

[138] Luke YL 1969 *The Special Functions and their Approximations* (Academic Press, New York)

[139] Buchholz H 1969 *The Confluent Hypergeometric Function* (Springer-Verlag, Heidelberg)

[140] Abad J and Sesma J 1995, Computation of the Regular Confluent Hypergeometric Function, *Mathematica J.* **5** 74-76

[141] Abad J and Sesma J 1997, A new expansion of the confluent hypergeometric function in terms of modified Bessel functions, *J. Comput. Appl. Math.* **78** 97-101

[142] Temme NM 1983, The Numerical Computation of the Confluent Hypergeometric Function U(a,b,z), *Numer. Math.* **41** 63-82